Accepted Manuscript

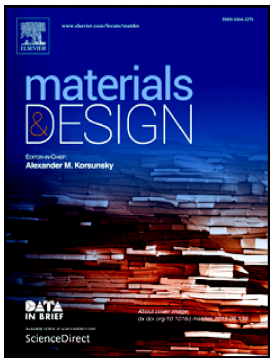

A new approach to rapidly generate random periodic representative volume elements for microstructural assessment of high volume fraction composites

Geng Li, Farzad Sharifpour, Aram Bahmani, John Montesano

PII: S0264-1275(18)30301-0
DOI: doi:10.1016/j.matdes.2018.04.031
Reference: JMADE 3844

To appear in: *Materials & Design*

Received date: 19 February 2018
Revised date: 10 April 2018
Accepted date: 11 April 2018

Please cite this article as: Geng Li, Farzad Sharifpour, Aram Bahmani, John Montesano , A new approach to rapidly generate random periodic representative volume elements for microstructural assessment of high volume fraction composites. The address for the corresponding author was captured as affiliation for all authors. Please check if appropriate. Jmade(2017), doi:10.1016/j.matdes.2018.04.031

A new approach to rapidly generate random periodic representative volume elements for microstructural assessment of high volume fraction composites

Geng Li [a,b], Farzad Sharifpour [a], Aram Bahmani [a], John Montesano [a] *

[a] Department of Mechanical and Mechatronics Engineering, University of Waterloo, 200 University Ave. West, Waterloo, N2L 3G1, Canada

[b] College of Advanced Interdisciplinary Studies, National University of Defense Technology, 137 Yanwachizhengjie Street, Changsha, Hunan, 410073, China

[*] Corresponding Author: Email address: john.montesano@uwaterloo.ca (J. Montesano)

Abstract

An algorithm based on event-driven molecular dynamics theory was developed to rapidly generate periodic representative volume elements (RVEs) with nonuniform distributions for both unidirectional fiber-reinforced and spherical particle-reinforced composites. Detailed statistical analyses were conducted for assessing the ability to generate RVEs with nonuniformly dispersed microstructures and either constant or random inclusion sizes for a wide range of volume fractions. The generated microstructures were directly compared with available microstructural optical images of a composite material, showing excellent statistical correlation and providing validation for the developed RVE generation approach. For further validation, finite element analysis was conducted using the generated RVEs in order to evaluate volume averaged elastic constants. The expected isotropic characteristics of the RVEs were correctly calculated, and excellent correlations with experimental data from the literature provided additional support for the algorithm accuracy. The versatile algorithm can rapidly generate RVEs with realistic reinforcement dispersions and high volume fractions up to 80%, which is advantageous compared to other algorithms. The proposed algorithm can be used as a design tool to accurately evaluate and tailor the mechanical properties of distinct composite material systems, and for their microstructural assessment including local damage predictions.

Keywords: Polymer-matrix composites (PMCs), High volume fractions, Computational micro-mechanics, Representative volume element (RVE) generation, Nonuniform reinforcement dispersion, Event-driven molecular dynamics

1. Introduction

Particulate- and fibre-reinforced composite materials have been extensively investigated due to their excellent mechanical and thermal properties, including high specific strength and stiffness, wear resistance, and tailorable coefficients of thermal expansion and thermal conductivity. Prior to designing a specific material system and optimizing corresponding structural components, the effective properties of composites can be evaluated through so-called computational experiments using a representative volume element (RVE) [1]-[7]. An RVE is an accurate depiction of the material's microstructure that is used to evaluate its effective macroscopic properties, thereby minimizing experimental testing during the early stages of design. An advantage with RVEs and related computational assessments is that the anisotropy of the composite material system can be directly tailored, and accurate microstructural assessments can be realized.

Similar to an RVE, a periodic unit cell (PUC) model can also be used to evaluate properties of composite materials. PUCs have simplified structured patterns for the reinforcement phase and often adopt symmetric boundary conditions [8]-[10]. In practice, however, composite microstructures are rarely structured, thus PUC models may not be suitable for assessing their 3D mechanical properties [11]-[13]. In addition, the evolution of microstructural parameters for materials involving plasticity or evolving microscopic damage are often not of a structured nature, thus PUC methods may not be suitable for these problems since the implication that all regions of the material are damaged simultaneously is not realistic.

Oh and Jin [14], [15] found that RVEs of unidirectional fibre-reinforced composites with random fibre arrangements, especially for high fibre volume fractions (HFVFs), resulted in variations in strain at fibre/matrix interfaces [14] and residual thermal stresses [15]. Gusev *et al.* [16] also found that the nonuniform microstructural fibre dispersion of a unidirectional glass/epoxy composite had significant influence on its transverse elastic properties. Recently, Ghayoor *et al.* [17] found that local stress values were more variable in nonuniform microstructures when

compared to periodic microstructures, and more likely to cause a disturbance of the load and stress distribution in the composite. Thus, to accurately assess the 3D mechanical properties and microstructural parameters of practical composites with high volume fractions, including predicting localized damage progression, it is important to generate realistic RVEs with random nonuniform reinforcement dispersions.

Several research efforts have been devoted to generating RVEs using random distribution algorithms (RDAs) for composite materials. The classical approach of RDAs is the so-called hard-core model (HCM), which assesses the position of newly generated random fibres to avoid overlaps [18], [19]. Due to the jamming limit with HCM algorithms, close packing [20], stirring, [21], [22], random sequential expansion (RSE) [23], and random sequential absorption (RSA) [24]-[26], algorithms have also been studied. Nonetheless, generating RVEs with higher fibre volume fractions in reasonable computational times remains challenging with these algorithms [27]. To overcome this limitation the nearest neighbour algorithm (NNA) [28] and modified NNA (MNNA) [29] were proposed, where random RVEs were generated with comparatively short computational times using nearest neighbour distribution functions. Recently, the elastic collision algorithm (ECA) was also proposed to generate RVEs with random fibre distributions [30]. After defining an initial fibre unit velocity for all fibres along a random direction, fibres displaced under an elastic collision law. However, the disturbance time interval is difficult to adjust for different volume fractions making the ECA impractical.

A new efficient method for generating RVEs for HFVF composites utilizes the principles of molecular dynamics (MD) which involves tracking inter-particle interactions [31], and has been successfully applied to generate 2D RVEs of rigid disks with high volume fractions [32], [33]. One of the limitations with time-driven MD (TDMD) or random walking algorithms (RWA) is that they require small time-steps and integration of the equations of motion [34]. Donev *et al.* [35] presented a more rapid event-driven molecular dynamics (EDMD) algorithm which is suitable for high

volume fractions without compromising accuracy. EDMD approaches schedule the sequence of the events that are predicted to occur in the future based on the present particle trajectories [36]. However, these algorithms can be difficult to implement, and the degree of nonuniformity for the resulting RVEs was not assessed in the reported studies. Recent work by Canalotti [37] has developed a new algorithm aimed to generate RVEs, and is among the first to do so for RVEs of composite materials containing HFVFs.

Although the above numerical approaches have made significant contributions toward generating practical RVEs for composite materials, accurate and efficient generation of nonuniformly distributed RVEs for composites with HFVFs remains a challenge. In this study, a simple and efficient algorithm was developed to generate RVEs for composites with high reinforcement volume fractions. The developed algorithm is based on EDMD theory and utilizes the open-source software DynamO [38] to randomly generate nonuniform reinforcement coordinates for RVEs with specified volume fraction in a few minutes or several seconds. Bahmani et al. [39] utilized this method to generate non-uniformly distributed three-dimensional RVEs for continuous unidirectional fiber composites with constant fiber radius. Thus, the goal of this study was to generate RVEs with non-uniformly distributed particles of random size. The corresponding statistical assessment of the RVE reinforcement nonuniform dispersion was performed to determine the effectiveness of the algorithm, and includes validation with available microstructural optical images of a composite material. A subsequent aim was to use the generated RVEs for developing finite element micromechanical models using custom scripts in the commercial software Abaqus. The mechanical properties of the composite materials studied were determined, with the goal of providing additional validation for the developed RVE generation algorithm. Both unidirectional fibre-reinforced and particulate-reinforced composites with high reinforcement volume fractions were studied in order to showcase the versatility of the developed algorithm, and its ability to overcome the different challenges when generating RVEs for distinct materials.

2. Development of EDMD-based algorithm for RVE geometry generation

2.1 Event-driven molecular dynamics overview

In recent years, MD simulations based on time-stepping algorithms have been broadly used for simulating the mobility of molecules or atoms for various material systems. For particular cases, including the present study, capturing the key features of interactions between particles is required. Thus, the EDMD approach is more suitable for simulating discrete interaction potentials, with the ability to provide quantitative predictions [40], [41]. Fig. 1 illustrates the conceptual difference with respect to interacting particles between conventional time-stepping MD and EDMD methods.

Considering two particles i and j with a relative separation distance σ, a discontinuity crossing (i.e., event) is expressed as a search for the roots of an overlap function:

$$f(t) = \left|r_i(t) - r_j(t)\right| - \sigma, \tag{1}$$

where $f(t)$ is a measure of the distance from a discontinuity in the potential, $r_i(t)$ and $r_j(t)$ are the positions of the two particles. In order to solve for the event impulse, ΔP, the appropriate solution to the conservation of energy (and momentum) equation is required:

$$\frac{1}{2}m_i\boldsymbol{v}_i^2 + \frac{1}{2}m_j\boldsymbol{v}_j^2 + \Delta U = \frac{1}{2}m_i\left(\boldsymbol{v}_i + \frac{\Delta P}{m_i}\right)^2 + \frac{1}{2}m_j\left(\boldsymbol{v}_j + \frac{\Delta P}{m_j}\right)^2. \tag{2}$$

Here, ΔU is the change in internal energy due to the discontinuity, m_i and m_j are the particle masses, and v_i and v_j are their velocities. The main objective is to track a series of event impulses and the resulting particle locations; further details can be found in Refs. [40], [41].

2.2 Generation of periodic RVEs with random reinforcement distribution

In this study, the EDMD open source software DynamO was used within a customized algorithm to generate periodic RVEs with nonuniform distributions for two types of composite materials, namely unidirectional fibre-reinforced and particulate-reinforced composites. Within DynamO, each particle is initially assigned a random velocity vector and an event table is automatically

generated which defines all potential collisions between particles in the RVE space (see Refs. [40], [41] for full details). Thus, a realistic random particle distribution is effectively guaranteed for all particle regions, with a significantly reduced computational time. Fig. 2 represents the algorithm flowchart for the generation of random RVE microstructures. Two cases were considered: (*i*) a 2D arrangement of circular fibres representing the cross-section of a continuous unidirectional fibre-reinforced composite; (*ii*) a 3D arrangement of spherical particles representing a particulate reinforced composite. The detailed 4-step procedure outlined in Fig. 2 is described subsequently.

The first step in using the algorithm involved preparing the input for the procedure, including the RVE size and reinforcement dimensions which can be constant or vary randomly depending on the script code (see Fig. 2). For unidirectional continuous fibre-reinforced composites the 2D cross-section perpendicular to the fibres defined the simulation space, while for particulate-reinforced composites a 3D RVE model was required. During the subsequent step the simulation was initialized using the input values, which included defining the number of fibres/particles, collision times or events, and the initial position of the fibers/particles [39] - [41].

The third step required performing necessary operations within DynamO to generate the particle output coordinate files. For generation of 2D periodic random fibre RVEs, the concept of gravity was used. First, the constant radius spheres were packed in a 3D simulation space, then the spheres were released and allowed to "fall down" to a 2D plane or "floor" (see Fig. 3). The boundary constraints of the simulation floor along the in-plane directions were configured to generate the desired periodic RVE geometry. In order to control the periodic particle distribution along one direction, a "wall" type constraint was used to define the boundary of the simulation space. Fig. 3 illustrates periodic constraints applied along the X-direction where particles can transfer randomly within the floor plane from one side to the other and particles can only cross the boundaries perpendicular to the X-direction. For generating RVEs with periodic geometry along both X and Y directions, the wall constraints were not required such that particles were allowed to freely cross all

boundaries. The total number of events were adjusted to control the total computational time, where for a personal computer with 3.4 GHz processor and 16 GB RAM, 100,000 events required approximately 10s on average to converge.

For the generation of 3D RVEs for particulate-reinforced composites, all particles during the simulation moved under standard Newtonian dynamics without the influence of external forces. Based on the same rules for the 2D RVE simulations, the configuration file was defined to set the initial number and the sizes of spheres. Fig. 4 shows the results of three configuration steps. For high volume fraction RVE generation, a high density configuration using a linear compression algorithm [42] was utilized to decrease the computational time further. Through use of this method, a 3D periodic random RVE with 65% reinforcement volume fraction was generated in approximately 20 seconds.

The final step (see Fig. 2) involved transforming the particle coordinates from the generated output file in step 3 to the commercial finite element software ABAQUS, and adjusting the RVE geometry to generate the proper periodic geometric model for subsequent finite element analysis. For high volume fraction simulations, there are more opportunities for particles to be in contact during RVE generation, however, in reality a small gap between fibres always exists due to very low but tangible particle crimp [22]. At the same time, contact between particles will lead to very small elements in FEA, which also causes unnecessary computational time or failure of convergence during analysis. Consequently, the minimum distance between particles in the developed algorithm was limited to 0.25% of the particle diameter. Furthermore, Python scripts were used to generate the solid model of the 2D RVEs and to ensure that periodic geometries were maintained, where two examples with single direction periodic boundaries are shown in Fig. 5 (one with constant diameter fibers and the other with variable diameter fibers). For the generated 3D RVEs, the spherical particles crossed all the face and edge boundaries, and customized Python scripts were used to ensure a 3D periodic geometry was maintained within the RVE. An example of

a generated RVE with random particle distribution and periodic geometry along all directions is shown in Fig. 6.

3. Spatial statistical assessment of generated RVEs

Statistical analysis was conducted for the generated RVE geometries in to asses the spatial distributions of the reinforcements and to verify their degree of nonuniformity. The corresponding results are presented in the subsequent sections.

3.1 2D continuous fibre-reinforced composite RVEs

For the continuous unidirectional fibre-reinforced composites considered, the size of the RVE was $150 \times 150 \mu m$ and the fibre diameter was 6 μm, resulting in approximately 400 – 520 fibers within the RVE depending on the fiber volume fraction. Note that the size of the RVEs were chosen in order to allow for a statistically accurate microstructural representation of the material system and a means to analyze its elastic response, and relative to reported studies on RVE size generation are deemed sufficiently large [43], [44].

First, a radial distribution function (RDF) was used to assess RVEs with fibre volume fractions ranging from 10% to 80% having constant diameter fibers. The RDF, $g(r)$, describes the density deviation as a function of distance from a reference fibre, allowing for assessment of the degree of nonuniform distribution, and was calculated using the following averaging equation [45]:

$$g(r) = \frac{2V}{N(N-1)} \frac{1}{V_r} \sum_{i=1}^{N} \sum_{j=1}^{i-1} \theta(r_{ij} - r)\theta(r + \Delta r - r_{ij}), \quad (3)$$

where r_{ij} is the distance between particles i and j, N is the number of particles, and $N(N-1)/2$ represents a weighting term. The term V is the volume (or area in 2D) of the region, $V_r = \pi(2r + \Delta r)\Delta r$ is the area of the annulus with inner radius r and width Δr, and the function $\theta(x)$ is given by

$$\theta(x) = \begin{cases} 1, & if\ x > 0 \\ 0, & if\ x \leq 0' \end{cases} \quad (4)$$

The product $\theta(r_{ij}-r)\theta(r+\Delta r-r_{ij})$ is 1 if particles i and j are within a distance between r and $r+\Delta r$ of each other, and 0 otherwise. When N increases $g(r)$ tends to 1 as r becomes sufficiently large, and periodic boundaries are considered to ensure that when r tends to infinity, the RDF is 1.

For different fibre volume fractions, Fig. 7 shows a plot of $g(r)$ with respect to normalized r which is obtained by multiplying the distance by RDF $\times\, 2/(N-1)$. The rightmost $g(r)$ curve with sharp peaks in Fig. 7 demonstrates the consistency of the distances between fibres in the RVE and thus a structured fibre arrangement, which was also observed for 80% fibre volume fraction and expected since the fibres are closely packed. For fibre volume fractions below 70% the magnitudes of the fluctuations were notably smaller, and the RDF values are more consistent which indicates a consistent nonuniform fibre distribution as shown in the RVE images in Fig. 7. For fibre volume fractions below 20%, $g(r)$ showed more variances with increasing r since the randomly distributed fibres were not consistent and the RVE contains matrix-rich regions. The radial distribution for complete fibre nonuniformity in the RVE will have a $g(r)$ tending to 1 when the radius of the annuli is increased, which is the case for the generated RVEs with fibre volume fractions below 70%, and representative of observed fibre distributions for unidirectional composites.

In order to validate the statistical assessment and the accuracy of the microstructural representation of the generated RVEs, a comparison of the RDF was made with a fabricated unidirectional fibre-reinforced composite from the study by Vaughan [28]. Based on Fig. 8a, the average fibre diameter was 6.6 μm and the fibre volume fraction was approximately 59.2%. ImageJ [46] was used to extract the center coordinates of the fibres (see Fig. 8b), and the RDF was calculated based on the pixel distance as shown in Fig. 8c (red curve). The blue curve in Fig. 8c shows the RDF of generated nonuniform distribution with 60% fibre volume fraction, demonstrating a strong correlation with the experimental result which also tends to 1 with the increasing of the distance of the annuli. Note that the jump in RDF at a lower distance in the blue

curve of Fig. 8c is caused by the minimum distance between two fibres, which should be larger than the diameter of the fibres in simulation.

In order to provide additional statistical assessment of the dispersion of fibers within the RVEs, Voronoi tessellations were computed using functions provided by the commercial software Matlab [47]. These routines create cells around each individual fiber center point which represents the area in space that is closer to that point than any other point. The edges of each cell are perpendicular to the connection of two near neighbors in the Voronoi tessellation. Fig. 9 demonstrates the Voronoi tessellations of the centers of the fibres in random distribution fibre with different volume fractions. From Fig. 9, all the axes are normalized to (0,1) and we can clearly see that the densities increase with increasing fibre volume fraction. For 62% volume fraction, the arrangement of the fibres are almost structured while for lower volume fraction distributions clusters in some regions are observed.

In order to be more consistent with the real composites, RVEs with random fiber diameters were generated using the EDMD-based algorithm, and the nearest neighbour distance distributions were applied to assess this method. It should be noted that the variation in fiber diameter considered was from 80-100% of the constant diameter. Fig. 10 shows the nearest neighbour distances of the 2D RVE with the same size in the blue histogram and random sizes in the red one. The blue curve and red dash curve are the fit curves of these two distributions respectively. For the RVEs with same size fibers the nearest neighbour distance has a lower limitation, while for the random size the histogram is bilateral. Figure 10 demonstrates the robustness of the random distribution EDMD-based method.

3.2 3D particulate-reinforced RVEs

For the particulate-reinforced composites the 3D RVEs were $200 \times 200 \times 200 \mu m$ in length, with a constant spherical particle diameter of 19 μm, resulting in more than 400 particles within the

RVE (depending on the inclusion volume fraction), and a statistically accurate microstructural representation of the material system. The generated particle volume fractions included 30%, 40%, 50%, and 60%. The spatial statistical metric considered in this study were near neighbour analysis, Voronoi domain analysis and 3D autocorrelation analysis to assess the degree of nonuniformity for the generated RVEs.

3.2.1 Near neighbour analysis in 3D

The commonly used functions for 3D spatial distribution analysis are *K*, *F*, and *G* functions [48], which are based on the near neighbor distance. The *K*-function in three dimensions is defined as:

$$K(r) = \frac{|B|}{n^2}\sum_{i=1}^{N}\sum_{j\neq i}\frac{I(\|x_i - x_j\| \leq r)}{w(i,j)} \tag{5}$$

where $I(\cdot)$ equals to 1 when the condition in the brackets is satisfied and the edge effect corrections is described by $w(i,j)$, which indicates the fraction of the circumference of the ith particle with radius $\|x_i - x_j\|$ within the RVE cube. For the complete spatial randomness (CSR) distribution, the *K*-function equals to $4\pi r^3/3$.

The *F*-function is an empty space function which represents the distance from each grid point to the nearest observed point as follows:

$$F(r) = \frac{1}{g}\sum_{i=1}^{g} I(d_i \leq r) \tag{6}$$

A fine grid in the RVE cube is set for estimating the *F*-function and d_i is the distance of the ith grid point to the nearest point. For the CSR distribution, the theoretical *F*-function is $1 - exp(-4\lambda\pi r^3/3)$, where λ is the intensity of uniform Poisson process, which represents the probabilities for random points in time for a process.

Instead of measuring the distance of grid point and its nearest point, the *G*-Function directly uses the distance of i^{th} point to the nearest point.

$$G(r) = \frac{1}{n}\sum_{i=1}^{n} I(d_i \leq r) \quad (7)$$

The theoretical *G*-function of CSR is $1 - exp(-4\lambda\pi r^3/3)$.

Figure 11 (a), (b) and (c) show these three spatial distribution functions for RVEs with 30% and 60% volume fractions, illustrating that the cumulative density recovery profiles of random distribution in RVEs with different fibre volume fractions are approximately the same. The Poisson distribution of particles which is shown by red dash line is also compared with the generated random distributions depicted by the blue solid lines. For higher fibre volume fraction the *K*-function shows disturbance around the Poisson distribution, while for lower volume fraction the generated random distribution correlates very well with the Poisson distribution. A close correlation between the *K*-function of the generated random and Poisson distributions implies that the generated RVE has greater degree of randomness and thus is a closer representation of a practical unidirectional fiber-reinforced composite. This is further confirmed by the *F*-function in Fig. 11(b) which also shows a good correlation with the Poisson distribution. The *G*-function of the generated RVEs with different fibre volume fractions are shown in and 60% fibre volume fractions.

According to Fig. 11 (a) and (c), where for an increase of volume fraction the spatial distributions deviate more from the CSR. Since the random distribution were generated with solid spherical particles instead of points, the *G*-function shows a jump from the distance of 19 μm, which is the diameter of the particles.

3.2.2 Voronoi domain analysis

The Voronoi tessellation in 2D is defined as a set of polygon areas surrounding each point (i.e., fibre center), where all points in the corresponding region of the specific point is closer to that point than to any other. For 3D application, such a Voronoi tessellation is defined by a set of polyhedron in which every point is closer to the corresponding point than to any of its neighbours. These

polyhedrons are also called Voronoi domain. In order to demonstrate the anisotropies of the random distribution, Voronoi Domain Direction Vectors (VDDV) here are used by means of summing the area weighted vectors of each facet of the polyhedrons [48].

In Fig. 12, VDDVs are described along with the histograms of the population components. For 30% and 60% volume fractions of the generated random distributed RVEs, the VDDVs are showing randomness very well in the left two vector diagrams. The *x*, *y* and *z* components of each VDDV have an even probability distribution between -1 and 1 as seen in the right two histograms, which further shows that the randomness of RVEs with the presented fibre volume fractions are well generated.

3.2.3 3D Autocorrelation analysis

Three-dimensional autocorrelation analysis describes the relative position of each particle in a region relative to every other particle, and not only to the nearest particles. A 3D autocorrelation diagram is depicted by taking one particle as a reference and plotting the relative positions of all other particles within a spherical region. This region is composed of many layers, and within each layer the density of particles is used to define density recovery profile, DRP (see Ref. [49], [50] for details).

The leftmost plots in Fig. 13a and b show the 3D autocorrelation analysis DRPs, in a distance distribution, for RVEs with randomly distributed particles and 30% and 60% particle volume fractions, while the leftmost plot in Fig. 13c corresponds to an RVE with hexagonal distribution and 30% volume fraction. The remaining plots in Fig. 13 present distance distributions and two direction distributions of the random particles relative to the reference particle (i.e., azimuthal angle, theta, and elevation angle, phi), which make up the spherical coordinate autocorrelation tri-histogram plots. The constant DRP values at an average magnitude within the spherical region for Fig. 13a and b demonstrate that these RVEs have consistent nonuniformly distributed particles,

while for Fig. 13c there is a clear variation of DRP within the region. The deviation from the average value of density may represent particle clustering (i.e., increased value) or low density zones.

For the direction distribution analysis shown in Fig. 13a and b, the generated RVEs have consistent particle densities in all radial directions for both the theta and phi angles, which is represented by circles with smooth edges. This further implies that the particles in these RVEs have consistent nonuniform random distributions. In contrast, for the RVE with hexagonal particle distribution the theta angle and phi angle have some peaks in the plots.

4. Mechanical property assessment of generated RVEs

A high-fidelity assessment of the mechanical properties of composites was the main motivation for developing an algorithm to randomly generate realistic RVEs with nonuniformly distributed reinforcements. Accordingly, the degree of RVE nonuniformity, and thus the reliability of the developed EDMD-based algorithm, can be examined further by evaluating mechanical properties for both unidirectional fibre-reinforced and particulate-reinforced composites. For this purpose, the commercial FEA software ABAQUS was utilized and the predicted values of the engineering constants along different material directions were compared for both materials.

4.1 Material description

The continuous E-glass fibre-reinforced Epikote 828/NMA/BDMA (100:60:1) epoxy system assessed by Tong *et al*. [51] was considered in this study. For the unidirectional fibre-reinforced glass/epoxy composite, the constituent isotropic elastic properties were determined by approximating typical values for E-glass fibers and epoxy resins found in the literature [52], [53]. The resulting constituent property values were $E_{1f} = 72\text{GPa}$, $E_{1m} = 3.35\text{GPa}$, $\nu_{12f} = 0.21$, and $\nu_{12m} = 0.35$,

and were used for analysis of both the glass fiber/epoxy and glass particle/epoxy composite. RVEs with various volume fractions were analyzed for both composites materials studied. It should be noted that although the random RVEs generated all had periodic geometries (see Figs. 5 and 6), periodic boundary conditions were not applied for FEA where instead symmetric boundary conditions were used for simplicity.

4.2 Numerical micromechanical finite element analysis

4.2.1 Continuous unidirectional glass fibre-reinforced/epoxy composites

It was assumed that the unidirectional glass fibre-reinforced/epoxy composites undergo linear elastic plane strain deformation when loaded in tension along the transverse fibre directions, thus the generated 2D RVEs were considered for obtaining the transverse elastic response of the composite. The square shaped RVEs had lengths of $500\,\mu m$ and randomly distributed fibres with $20\,\mu m$ diameter (initially constant). Three-node linear plane strain elements (i.e. CPE3) were used to mesh each RVE, and it was assumed that the fibres and matrix are perfectly bonded. In order to evaluate the composite transverse modulus, E_{22}, and the Poisson ratio ν_{23}, a horizontal strain of 0.5% was applied to the right side of the RVEs, while for evaluation of E_{33} and ν_{32} a vertical strain of 0.5% was applied to the top side of the RVEs (see Fig. 14). Well-known volume averaging techniques [52], not included here for brevity, were used to evaluate the elastic constants. For the 2D model area averaging is equivalent to volume averaging since the reinforcement fibers are continuous. Furthermore, assuming a linear elastic response the volume averaged modulus can be written in terms of volume averaged stress and the corresponding volume averaged strain, while the corresponding Poisson's ratio is evaluated as follows:

$$E_{kk} = \frac{\sum_{i=1}^{N} \sigma_{kk}^{i} A^{i}}{\sum_{i=1}^{N} \varepsilon_{kk}^{i} A^{i}},\ \nu_{jk} = -\frac{\sum_{i=1}^{N} \varepsilon_{kk}^{i} A^{i}}{\sum_{i=1}^{N} \varepsilon_{jj}^{i} A^{i}} \tag{8}$$

where N indicates the total number of elements in the RVE mesh, σ_{kk}^{i} and ε_{kk}^{i} respectively denote the normal stress and strain components for element i, and A^{i} is the area of element i.

Resultant normal stress distributions for a 2D RVE with 62% fibre volume fraction for both loading cases are depicted in Fig. 14, which illustrates that stress concentrations located at the fibre/matrix interfaces were aligned with the loading direction as expected. Also, the magnitude of the local normal stresses greatly depends on the distance between fibres, where maximum normal stresses resulted in regions with higher fibre concentrations as shown in Fig. 14. Using Eq. (8) and E_{22} as a metric, a mesh sensitivity analysis was performed with the 62% fibre volume fraction RVE to determine the appropriate element size for all RVEs analyzed. Fig. 15 demonstrates the effect of mesh size on E_{22}, which indicates that an element size lower than $30\ \mu m^2$ leads to a convergence of the results. For this study, an element size of $30\ \mu m^2$ was utilized for all 2D RVEs.

Table 1 presents the evaluated elastic constants for the RVE with $V_f = 0.62$. The predicted Young's moduli correlate better with the experimental data [53] in comparison to the Halpin-Tsai predictions [54], while the evaluated Poisson's ratios correlate well with experimental data for both cases. Furthermore, unidirectional fibre-reinforced composites typically exhibit transversely isotropic behaviour in accordance with Eq. (9), thus the consistency of the elastic properties in both transverse directions of the RVE can be used to assess the degree of nonuniformity of the fibres and provide another form of validation for the RVE generation algorithm.

$$E_{22} = E_{33}, \nu_{23} = \nu_{32}, \frac{\nu_{32}}{E_{33}} = \frac{\nu_{23}}{E_{22}} \tag{9}$$

As can be inferred from Table 1, the relations defined by Eq. (9) held for the RVE analyzed. These results highlight that the fibres have been ideally distributed in the RVE in both transverse directions, suggesting that the EDMD-based algorithm can generate practical RVEs.

To further demonstrate the capability of the algorithm to generate RVEs with nonuniform fibre distributions, five different RVEs with the same V_f = 62% were assessed. The evaluated volume

averaged transverse modulus for these RVEs is presented in Table 2, demonstrating consistency in the obtained results and stability of the EDMD-based algorithm.

Additional FEA was conducted for a number of similar RVEs with a wide range of fibre volume fractions (i.e. $V_f = 0.30, 0.40, 0.50, and\ 0.62$). The corresponding mechanical properties are shown in Table 3 along with predictions obtained using Halpin-Tsai expressions. These results reveal that the algorithm can randomly generate practical nonuniformly distributed RVEs since predicted E_{22} and E_{33} values for a specific fibre volume fraction are similar in magnitude, which was the main focus of the study. These results also highlight that the developed algorithm can generate consistent nonuniform randomly distributed RVEs over a wide range of fibre volume fractions. It should be noted that the predicted moduli have a notable discrepancy in comparison with those predicted using the Halpin-Tsai relation, which assumes a certain structured arrangement of fibres (i.e., not randomly distributed). A similar range of discrepancy was also reported by Pathan *et al.* [55].

In order to enhance the consistency of the FE model with real UD composites and further validate the RVE generation algorithm, additional simulations were performed on the RVEs with random diameter fibers for two high fiber volume fractions (i.e. $V_f = 0.50$ and 0.62). The calculated volume averaged transverse modulus for these models were compared to the constant diameter RVE models presented in Table 1 in Fig. 16. It is clear that the adverse consequence of inequality of fibre size can alter the elastic constant up to 10% for the E-glass/epoxy material considered in this study. It is worth noting that same volume fraction was obtained using two distinct fibre distributions.

4.2.2 Glass particle-reinforced/epoxy composites

The validity of the EDMD-based algorithm to randomly generate 3D periodic RVEs for nonuniformly distributed particulate-reinforced composites was also examined. Particles have been chosen instead of fibres here to test the capability of the algorithm in generating more complex geometries with distinct limiting conditions. In the analysis, cubic RVEs with length $200\ \mu m$ and

constant spherical particle diameter of $19\,\mu m$ with various particulate volume fractions were produced. Three-dimensional 4-node linear tetrahedron elements (i.e. C3D4) were utilized to mesh each RVE, and the particles were perfectly bonded to the matrix. The 3D linear elastic RVEs were subjected to normal strains of 0.5% along the principal directions in order to obtain the corresponding elastic constants. Similar to Eq. (8), now using volume averaged stresses and strains, the moduli and Poisson's ratios were evaluated using the following:

$$E_{kk} = \frac{\sum_{i=1}^{N} \sigma_{kk}^{i} V^{i}}{\sum_{i=1}^{N} \varepsilon_{kk}^{i} V^{i}},\ \nu_{jk} = -\frac{\sum_{i=1}^{N} \varepsilon_{kk}^{i} V^{i}}{\sum_{i=1}^{N} \varepsilon_{jj}^{i} V^{i}} \tag{10}$$

where V^{i} denotes the allocated volume of i^{th} element. Fig. 17 shows the Mises stress distribution for an RVE with 60% particle volume fraction under an applied uniaxial displacement. Similar to the 2D RVEs, the local stress concentrations was found to be greater in regions with higher particle packing, and the maximum stresses for both matrix and fibres were observed in the same regions.

The evaluated elastic constants for a wide range of particle volume fractions are presented in Table 4. The equivalency of E_{11}, E_{22} and E_{33} (and similarly $\boldsymbol{\nu_{12}}$, $\boldsymbol{\nu_{13}}$ and $\boldsymbol{\nu_{23}}$) for a specific volume fraction suggests isotropic behavior of the particulate composite in all principal material directions, which is expected since the particles are spherical in shape and nonuniformly distributed. These results demonstrate that for a particle-reinforced composite the developed RVE generation algorithm can generate consistent nonuniform randomly distributed particle distributions in three-dimensional space. Moreover, the algorithm can reliably generate periodic geometries for high volume fractions.

The stability of the algorithm in generating random RVEs with the same particulate volume fraction was also assessed by comparing the corresponding Young's moduli as shown in Table 5 for four particle volume fractions. The consistency of the results for a specific volume fraction further reveal the ability of the developed algorithm to generate truly random RVEs for various volume fractions ranging from low to high.

To analyze the repercussions of discrepancy between the particle diameter, the results from two volume fraction RVEs (i.e. $V_f = 0.30$ and 0.40) were compared to those obtained for the constant diameter RVEs from Table 4 in Fig. 18. Again, the significance of including a variable particle size on mechanical properties of the glass particle/epoxy composite studied is notable. It should be noted that in this figure the elastic moduli in one direction (i.e., E_{11}) were presented with the average of elastic modulus along the principal material directions.

5. Conclusions

An effective and versatile algorithm based on event-driven molecular dynamics theory was developed for rapidly generating random representative volume elements (RVEs) with nonuniformly distributed reinforcements with either constant or random sizes for two distinct types of composites, specifically unidirectional continuous fibre-reinforced and spherical particulate-reinforced. RVEs were generated with a range of reinforcement volume fractions up to 80%, which is an advantage over existing methods that require considerable computational resources and/or cannot converge for high volume fractions. The computational requirement to generate all the RVEs in this study was no more than 20 seconds on a stand-alone personal computer. Detailed statistical analyses were conducted to assess the uniformity of the reinforcement dispersions for the randomly generated RVEs. Comparisons with microstructures of actual composites from the literature demonstrated that the generated RVEs exhibit consistent nonuniform and realistic spatial dispersions, and provided validation for the developed RVE generation algorithm. Furthermore, finite element analysis was performed on the generated RVEs to provide additional validation for the developed algorithm. For the unidirectional fiber-reinforced composites analyzed, the evaluated RVE volume averaged elastic constants were equivalent in both transverse fibre directions for all volume fractions considered. Thus, the expected transversely isotropic response was confirmed which indicated that the nonuniform dispersion of fibers in the randomly generated RVEs was

indeed representative of the actual material. For the particulate-reinforced composites analyzed the evaluated elastic constants demonstrated an isotropic response along all principal directions, which further verifies the accuracy of the random RVE generation algorithm.

The validated results presented provide confidence in the ability of the developed algorithm to rapidly generate realistic RVEs with high reinforcement volume fractions for various types of composite materials. In practice, the algorithm can be used as a design tool to accurately evaluate and tailor the mechanical properties of distinct material systems for a specific structural application, and for accurate microstructural assessment including predictions of microscopic crack progression which requires RVEs with realistic nonuniformly dispersed reinforcements. Nevertheless, additional studies are required to extend the microstructural characterization of the materials considered and broaden the applicability of the developed algorithm. The algorithm can be applied to generate RVEs for aligned discontinuous fiber-reinforced composites with high fibre volume fractions, which are representative of emerging extruded or additively manufactured composites.

Acknowledgements

The authors thank the University of Waterloo for funding in support of this research. The first author acknowledges funding from the China Scholarship Council, while the second author acknowledges funding through an Ontario Graduate Scholarship.

References

[1] Wang ZQ, Wang XQ, Zhang JF, Liang WY, Zhou LM. Automatic generation of random distribution of fibers in long-fiber-reinforced composites and mesomechanical simulation. Mater Des 2011;32:885–891.

[2] Naya F, Gonzalez C, Lopes CS, Veen SV, Pons F. Computational micromechanics of the transverse and shear behavior of unidirectional fiber reinforced polymers including environmental effects. Compos Part A Appl Sci 2017;92(2017):146–157.

[3] Wang XQ, Zhang JF, WangZQ, Zhou S, Sun XY. Effects of interphase properties in unidirectional fiber reinforced composite materials. Mater Des 2011;32:3486–3492.

[4] Mahmoodi MJ, Aghdam MM, Shakeri M. Micromechanical modeling of interface damage of metal matrix composites subjected to off-axis loading. Mater Des 2010;31:829–836.

[5] Kirtania S, Chakraborty D. Multi-scale modeling of carbon nanotube reinforced composites with a fiber break. Mater Des 2012;35:498–504.

[6] Sohn DW. Periodic mesh generation and homogenization of inclusion-reinforced composites using an element-carving technique with local mesh refinement. Comp Struc 2018;192(2018):153–164.

[7] Montesano J, McCleave B, Singh CV. Prediction of ply crack evolution and stiffness degradation in multidirectional symmetric laminates under multiaxial stress states. Compos Part B Eng 2018;133(2018):53–67.

[8] Li S, Wongsto A. Unit cells for micromechanical analyses of particle-reinforced composites. Mech Mater 2004;36(7):543–572.

[9] Wongsto A, Li S. Micromechanical FE analysis of UD fibre-reinforced composites with fibres distributed at random over the transverse crosssection. Compos Part A Appl Sci 2005;36(9):1246–66.

[10] Li S. Boundary conditions for unit cells from periodic microstructures and their implications. Compos Sci Technol 2008;68(9):1962–1974.

[11] Krop S, Meijer HEH, Breemen LCA. Multi-mode modeling of global and local deformation, and failure, in particle filled epoxy systems. Compos Part A Appl Sci 2016;88(2016):1–9.

[12] Meguid SA, Shagai G, Paskaramoorthy R. On the local elastic–plastic behaviour of the interface in titanium/silicon carbide composites. Compos Part A Appl Sci 2002;33(12):1629–1640.

[13] Kammoun S, Doghn I, Adam L, Robert G, Delannay. First pseudo-grain failure model for inelastic composites with misaligned short fibers. Compos Part A Appl Sci 2011;42(12):1892–1902.

[14] Oh JH, Jin KK, Ha SK. Interfacial strain distribution of a unidirectional composite with randomly distributed fibres under transverse loading. J Compos Mater 2005;40(9):759–778.

[15] Jin KK, Oh JH, Ha SK. Effect of fibre arrangement on residual thermal stress distributions in a unidirectional composite. J Compos Mater 2007;41(5):591–611.

[16] Gusev AA, Hine PJ, Ward IM. Fibre packing and elastic properties of a transversely random unidirectional glass/epoxy composite. Compos Sci Technol 2000;60(4):535–541.

[17] Ghayoor H, Hoa SV, Marsden CC. A micromechanical study of stress concentrations in composites. Compos Part B Eng 2018;132(2018);115–124.

[18] Yang S, Tewari A, Gokhale AM. Modeling of non-uniform spatial arrangement of fibres in a ceramic matrix composite. Acta Mater 1997;45(7):3059–3069.

[19] Qing H. Automatic generation of 2D micromechanical finite element model of silicon–carbide/aluminum metal matrix composites: Effects of the boundary conditions. Mater Des 2013;44:446-453.

[20] Jodrey WS, Tory EM. Computer simulation of close random packing of equal spheres. Phys Rev A 1985;32(4):2347–2351.

[21] Melro AR, Camanho PP, Pinho ST. Generation of random distribution of fibres in long-fibre reinforced composites. Compos Sci Technol 2008;68(9):2092–2102.

[22] Romanov V, V. Lomov S, Swolfs Y, Orlova S, Gorbatikh L, Verpoest I. Statistical analysis of real and simulated fibre arrangements in unidirectional composites. Compos Sci Technol 2013;87(2013):126–134.

[23] Yang L, Yan Y, Ran ZG, Liu YJ. A new method for generating random fibre distributions for fibre reinforced composites. Compos Sci Technol 2013;76(2013):14–20.

[24] Babu KP, Mohite PM, Upadhyay. Development of an RVE and its stiffness predictions based on mathematical homogenization theory for short fibre composites. Int J Solid Struct 2018;130-131:80-104.

[25] Liu H, Zeng D, Li Y, Jiang L. Development of RVE-embedded solid elements model for predicting effective elastic constants of discontinuous fiber reinforced composites. Mech Mater 2016;93:109-123.

[26] Pan Y, Iorga L, Pelegro AA. Numercial generation of random chopped fiber composite RVE and its elastic properties. Compos Sci Technol 2008;68:2792-2798.

[27] Buryachenko VA, Pagano NJ, Kim RY, Spowart JE. Quantitative description and numerical simulation of random microstructures of composites and their effective elastic moduli. Int J Solids Struct 2003;40(1):47–72.

[28] Vaughan TJ, McCarthy CT. A combined experimental-numerical approach for generating statistically equivalent fibre distributions for high strength laminated composite materials. Compos Sci Technol 2010;70(2):291–297.

[29] Wang WZ, Dai YH, Zhang C, Gao XS, Zhao MY. Micromechanical modeling of fibre-reinforced composites with statistically equivalent random fibre distribution. Mater 2016;9(624):1–14.

[30] Zhang TT, Yan Y. A comparison between random model and periodic model for fibre-reinforced composites based on a new method for generating fibre distributions. Polym. Compos 2017;38(1):77–86.

[31] Alder BJ, Wainwright TE. Studies in molecular dynamics. I. general method. J Chem Phys 1959;31(2):459–466.

[32] Lubachevsky BD, Stillinger FH. Geometric properties of random disk packings. J Stat Phys 1990;60(5):561–583.

[33] Ghossein E, Levesque M. A comprehensive validation of analytical homogenization models: The case of ellipsoidal particles reinforced composites. Mech Mater 2014;75(2014):135–150.

[34] Zhang ZH, Song XG, Liu Y, Wu D, Song CM. Three-dimensional mesoscale modelling of concrete composites by using random walking algorithm. Compos Sci Technol 2017;149(2017):235–245.

[35] Donev A, Torquato S, Stillinger FH, Connelly R. Jamming in hard sphere and disk packings. J Appl Phys 2004;95(3):989–999.

[36] Sain R. Numerical simulation of pore-scale heterogeneity and its effects on elastic, electrical and transport properties. PhD thesis, Stanford University, 2010.

[37] Canalotti G. On the generation of RVE-based models of composites reinforced with long fibers or spherical particles. Compos Struct 2016;138:84-95.

[38] DynamO. http://dynamomd.org/, 2017 (accessed 13 November 2017).

[39] Bahmani A, Li G, Willett T, Montesano M. Three-dimensional microscopic assessment of randomly distributed representative volume elements for high fiber volume fraction unidirectional composites. Comp Struc 2018;192(2018):153–164.

[40] Bannerman MN, Sargant R, Lue L. DynamO: A free O(N) general event-driven simulator. J Comp Chem 2011;32(2011):3329–3338.

[41] Strobl S, Bannerman MN, Poeschel T. Stable algorithm for event detection in event-driven particle dynamics: logical states. Comput Part Mech 2016;3(3):383–388.

[42] Stillinger FH, Lubachevsky BD. Crystalline—amorphous interface packings for disks and spheres. J Stat Phys 1993;73(3-4):497–514.

[43] Savvas D, Stefanou G, Papadrakakis M. Determination of RVE size for random composites with local volume fraction variation. Comp Meth App Mech Eng 2016;305:340-358.

[44] Pathan MV, Tagarielli VL, Patsias S. Numerical predictions of the anisotropic viscoelastic response of uni-directional fibre composites. Compos Part A 2017;93:18-32.

[45] Visser PJ, Luding S, Srivastava S. Advanced Programming in Engineering lecture notes. https://www2.msm.ctw.utwente.nl/sluding/TEACHING/APiE_Script_v2011.pdf, 2017:48 (accessed 3 April 2018).

[46] ImageJ. https://imagej.nih.gov/ij/, 2017 (accessed 13 November 2017).

[47] Qiang D, Faber V, Gunzburger M. Centroidal Voronoi tessellations: applications and algorithms. Published by the Society for Industrial and Applied Mathematics 2017;41:637-76.

[48] Baddeley AJ, Moyeed RA, Howard CV, Boyde A. Analysis of a three-dimensional point pattern with replication. Appl Stats 1993;42:641–668.

[49] Rodieck RW. The density recovery profile: A method for analysis of points in the plane applicable to retinal studies. Vis Neurosci 1991;6(2):95–111.

[50] Eglen SJ, Lofgreen DD, Raven MA, Reese BE. Analysis of spatial relationships in three dimensions: Tools for the study of nerve cell patterning. BMC Neurosci 2008;9(68):1–7.

[51] Tong J, Guild FJ, Ogin SL, Smith PA. On matrix crack growth in quasi-isotropic laminates -I. experimental investigation. Compos Sci Technol 1997;57(11):1527–1535.

[52] Trias D, Costa J, Mayugo JA, Hurtado JE. Random models versus periodic models for fibre reinforced composites. Comput Mater Sci 2006;38(2):316–324.

[53] Soden P, Hinton M, Kaddour A. Lamina properties lay-up configurations and loading conditions for a range of fibre-reinforced composites laminates. Compos Sci Technol 1998;58(7):1225–1254.

[54] Halpin JC, Kardos JL. The Halpin-Tsai Equations: A Review. Polym Eng Sci 1976;16(5):344–352.

[55] Pathan MV, Tagarielli VL, Patsias S, Baiz-Villafranca PM. A new algorithm to generate representative volume elements of composites with cylindrical or spherical fillers. Compos Part B Eng 2017;110(2017):267–278.

Figure Captions

Fig. 1. Schematic of time-stepping method and event-driven algorithm.

Fig. 2. Algorithm flowchart for random RVE generation.

Fig. 3. RVE generation procedure for 2D randomly distributed fibres with X-direction periodic geometry by utilizing (a) same size and (b) random size.

Fig. 4. RVE generation procedure for 3D randomly distributed spherical particles with fully periodic geometry.

Fig. 5. Examples of generated 2D RVEs with randomly distributed fibres having periodic geometry along X-direction and $V_f = 0.62$.

Fig. 6. Generated 3D RVE with randomly distributed spherical particles and V_f = 30%.

Fig. 7. Radial distribution functions (RDF) for randomly distibuted 2D RVEs with different volume fractions, and structured rectangular distribution.

Fig. 8. (a) Experimental image of unidirectional composite cross-section from Ref. [28], (b) corresponding center coordinates of the fibres prossessed by ImageJ, and (c) comparison of radial distribution functions (RDF) for real transverse cross-section of unidirectional composite based on "pixel distance" with red curve, and for generated random RVE with blue curve.

Fig. 9. The Voronoi tessellation of the centers of fibres in random distribution for different volume fractions.

Fig. 10. Nearest neighbour distance distributions for 2D random particles generated by EDMD method with same size (blue histogram and blue fit curve) and random size (red histogram and red dash fit curve)

Fig. 11. Nearest neighbour distance distributions analyses for 3D random particles generated by EDMD method with (a) K-function, (b) F-function and (c) G-function

Fig. 12. Voronoi domain analysis of random distribution in 30% (a) and 60% (b) volume fractions by using Voronoi Domain Direction Vectors

Fig. 13. 3D Autocorrelation analysis and density recovery profile for RVEs with (a) 30% V_f and random distribution, (b) 60% V_f and random distribution, and (c) 30% V_f and structured hexagonal distribution.

Fig. 14. Normal stress distribution along loading directions for 2D RVEs with $V_f = 0.62$, (a) horizontal loading, and (b) vertical loading.

Fig. 15. Effect of mesh size on transverse Young's modulus for 2D RVE with $V_f = 0.62$.

Fig. 16. A comparison of volume averaged transverse elastic modulus for RVEs with constant diameter and variable diameter fibres, for a glass fiber/epoxy UD composite with $V_f = 0.50$ and 0.62.

Fig. 17. Mises stresses contours for 3D RVE with $V_f = 0.60$: (a) particles and (b) matrix.

Fig. 18. A comparison of volume averaged elastic modulus for RVEs with constant diameter and variable diameter particles, for a glass particle/epoxy composite with $V_f = 0.30$ and 0.40.

Tables

Table 1. Evaluated and experimental elastic constants for randomly distributed 2D RVE with $V_f = 0.62$.

	E_{22} (GPa)	E_{33} (GPa)	ν_{23}	ν_{32}
FEA	14.452	14.324	0.344	0.338
Halpin-Tsai	15.18	15.18	0.33	0.33
Experimental [51]	13	13	0.3	0.3
Error 1[a] (%)	4.79	5.64	7.5	5.62
Error 2[b] (%)	11.16	10.18	14.7	12.67

[a] Comparing FEA result with Halpin-Tsai formula
[b] Comparing FEA result with experimental data

Table 2. Evaluated transverse elastic modulus for randomly distributed 2D RVEs with V_f = 0.62% and different random geometries.

	Model 1	**Model 2**	**Model 3**	**Model 4**	**Model 5**
$\boldsymbol{E_{22}}$ **(GPa)**	14.45	14.38	14.14	14.64	14.98
Error 1 [a] **(%)**	0.46	0.95	2.6	0.84	3.18

[a] Results were compared with the average of these five models

Table 3. Evaluated elastic constants for randomly distributed 2D RVEs with different V_f.

V_f (%)	E_{22} (GPa)	E_{33} (GPa)	ν_{23}	ν_{32}	$\frac{E_{22}}{E_{33}}$	$\frac{\nu_{23}}{\nu_{32}}$	$\frac{E_{22}\nu_{32}}{E_{33}\nu_{23}}$
	FEM / Ref. [54]						
30 (1)	6.10/6.91	6.00/6.91	0.500/0.46	0.493/0.46	1.017	1.009	1.008
40 (2)	7.57/8.74	7.52/8.74	0.471/0.42	0.468/0.42	1.006	1.007	0.999
50 (3)	9.70/11.12	9.67/11.12	0.424/0.37	0.420/0.37	1.003	1.010	0.994
62 (4)	14.45/15.18	14.32/15.18	0.344/0.32	0.338/0.32	1.008	1.018	0.991
Error (%)	E_{22} (GPa)	E_{33} (GPa)	ν_{23}	ν_{32}	$\frac{E_{22}}{E_{33}}$	$\frac{\nu_{23}}{\nu_{32}}$	$\frac{E_{22}\nu_{32}}{E_{33}\nu_{23}}$
	FEM / Ref. [54]						
%Diff(1)	11.8	13.3	8.3	7.3	1.72	0.93	0.78
%Diff(2)	13.4	14.0	12.2	11.4	0.64	0.68	0.04
%Diff(3)	12.72	13.01	14.60	13.51	0.33	0.95	0.62
%Diff(4)	4.8	5.6	7.5	5.6	0.89	1.78	0.87

Table 4. Evaluated elastic constants for randomly distributed 3D RVEs with different V_f.

V_f (%)	E_{11} (GPa)	E_{22} (GPa)	E_{33} (GPa)	ν_{12}	ν_{13}	ν_{23}	$\frac{Max(E_{22})}{Min(E_{33})}$	$\frac{Max(E_{ii}-E_{jj})}{Avg(E_{kk})}$ (%)
30	5.907	5.903	5.927	0.324	0.326	0.32	1.004	0.41
40	8.274	8.321	8.352	0.314	0.312	0.302	1.009	0.37
50	10.349	10.138	10.417	0.292	0.2982	0.286	1.028	2.71
60	15.459	15.179	14.87	0.262	0.272	0.28	1.040	3.88

Table 5. Evaluated elastic modulus for randomly distributed 3D RVEs with different volume fractions and random geometries.

V_f (%)	$E_{11}^{1}{}^{*}$	$E_{11}^{2}{}^{*}$	$E_{11}^{3}{}^{*}$
30	5.907	5.941	5.942
40	8.056	8.274	8.139
50	10.349	10.864	10.704
60	15.301	15.537	15.459

* The superscripts correspond to the RVE model number.

Highlights

- Novel algorithm developed to rapidly generate RVEs with nonuniform reinforcement dispersions for high volume fraction unidirectional and particulate composites

- Statistical assessment of reinforcement dispersions reveal RVEs are representative of real microstructures, and validated by comparison with actual composite microstructures

- RVEs with volume fractions up to 80% were rapidly generated without convergence issues

- Computational microscopic assessment provided means to evaluate volume averaged mechanical properties, with excellent correlation to available experimental data

- Developed algorithm can be used as design tool to accurately evaluate and tailor properties of distinct composite materials

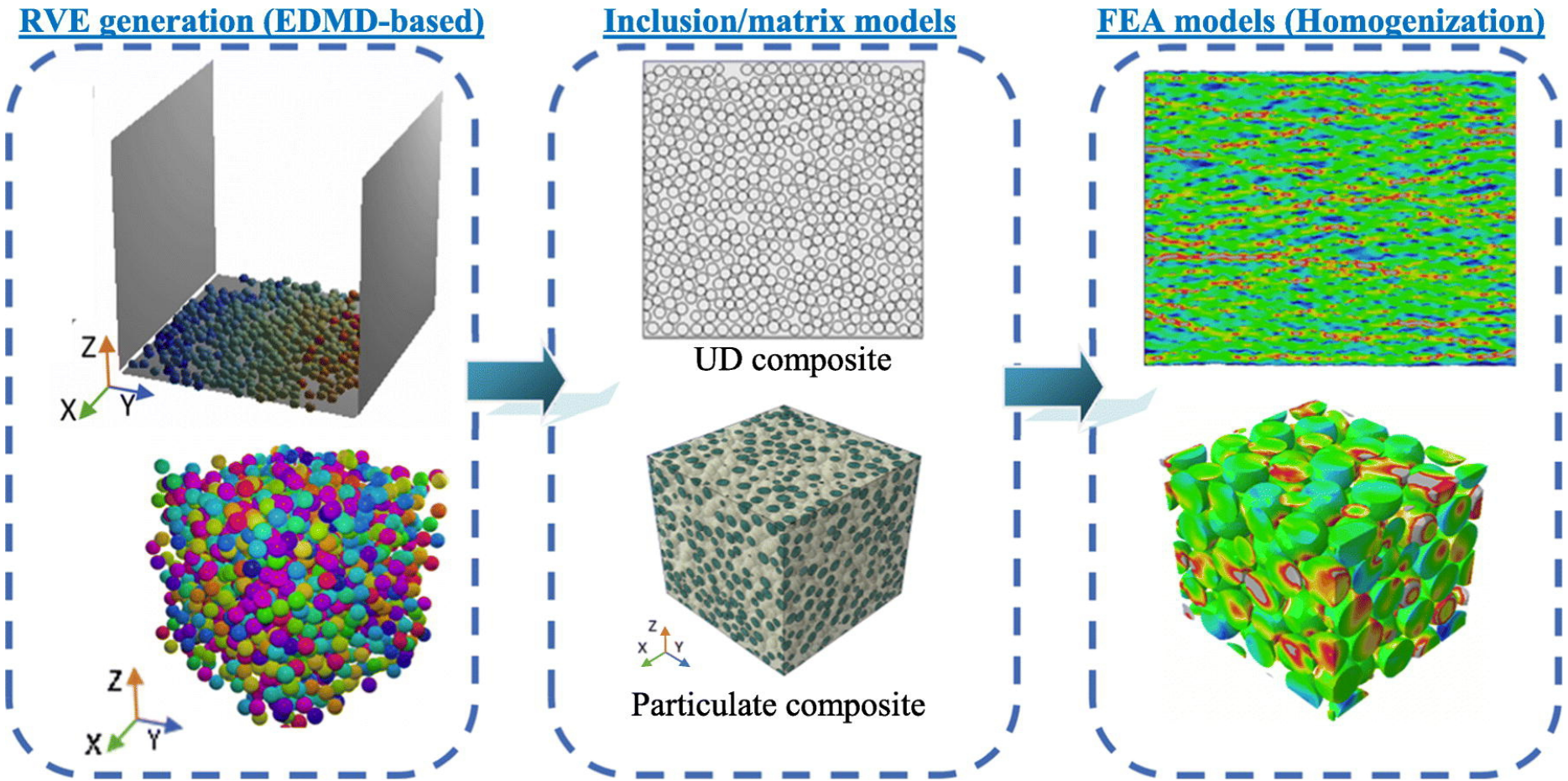

Graphics Abstract

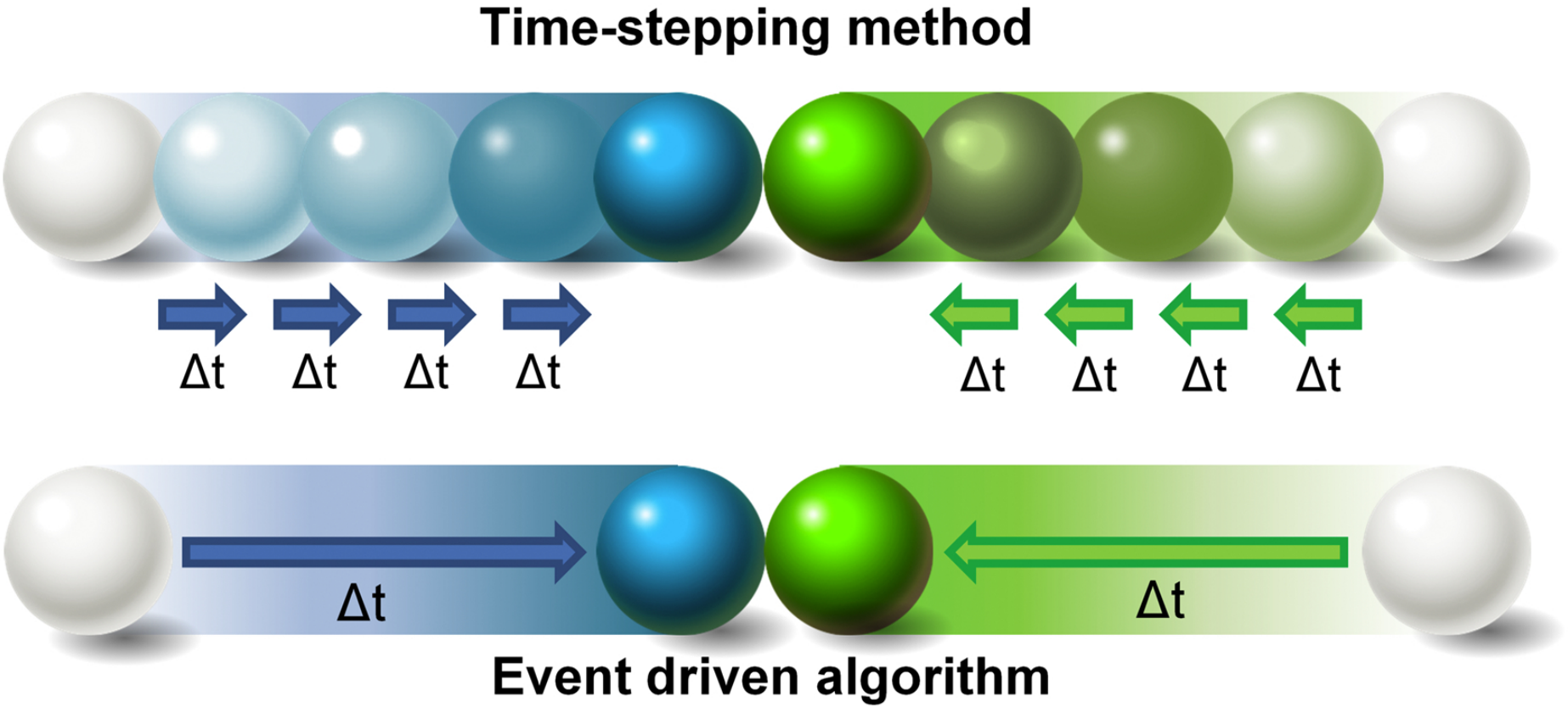
Time-stepping method
Δt
Δt
Δt
Δt
Δt
Δt
Δt
Δt
Δt
Δt
Event driven algorithm

Figure 1

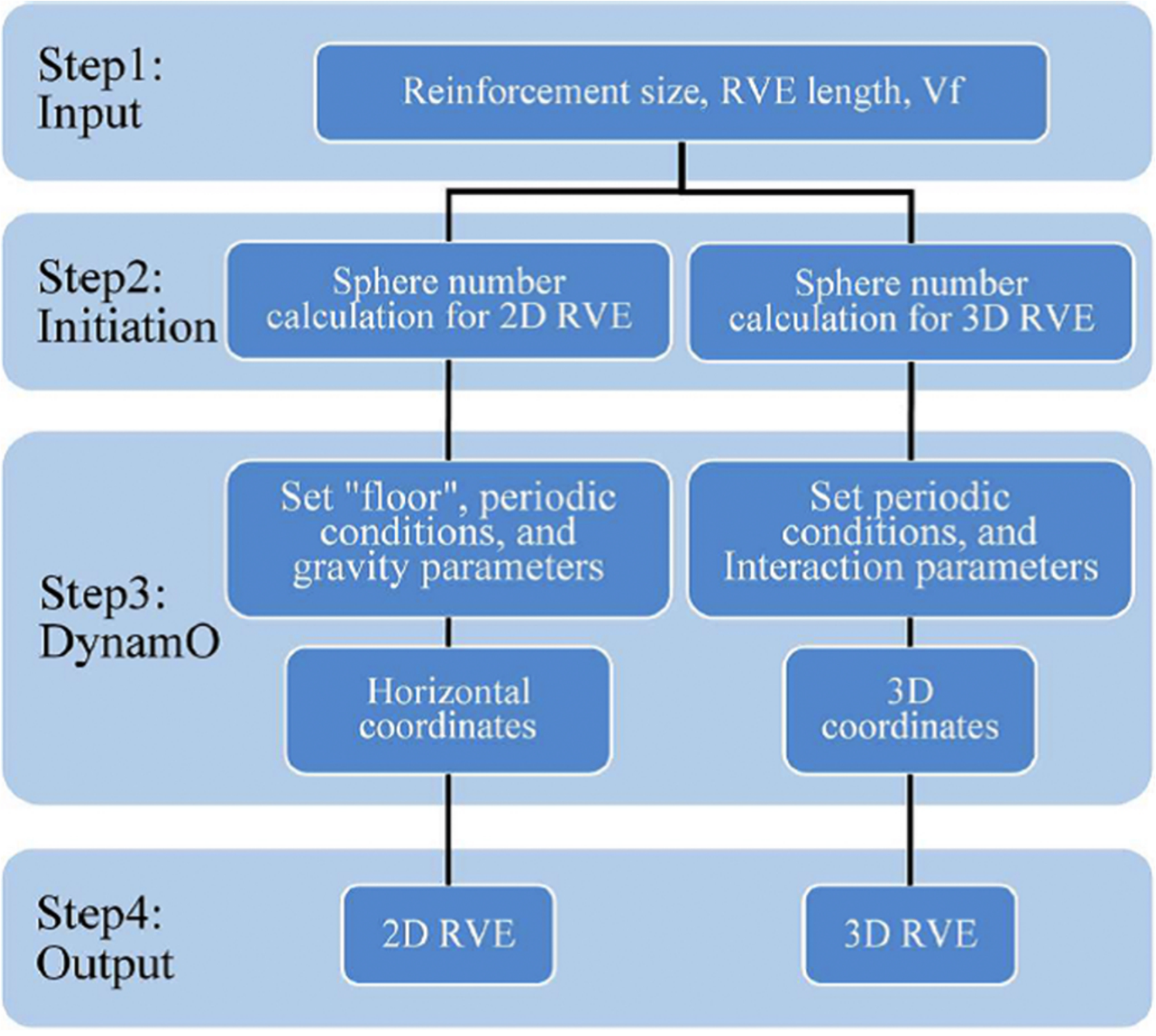
Step1:
Input
Reinforcement size, RVE length, Vf
Step2:
Initiation
Sphere number calculation for 2D RVE
Sphere number calculation for 3D RVE
Step3:
DynamO
Set "floor", periodic conditions, and gravity parameters
Set periodic conditions, and Interaction parameters
Horizontal coordinates
3D coordinates
Step4:
Output
2D RVE
3D RVE

Figure 2

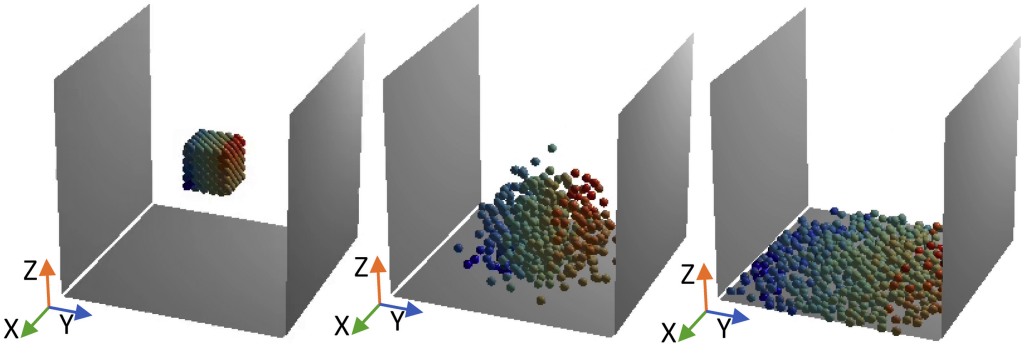

Figure 3

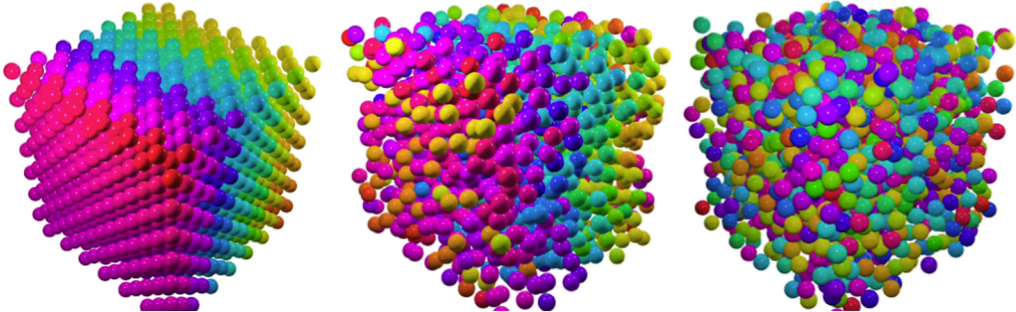

Figure 4

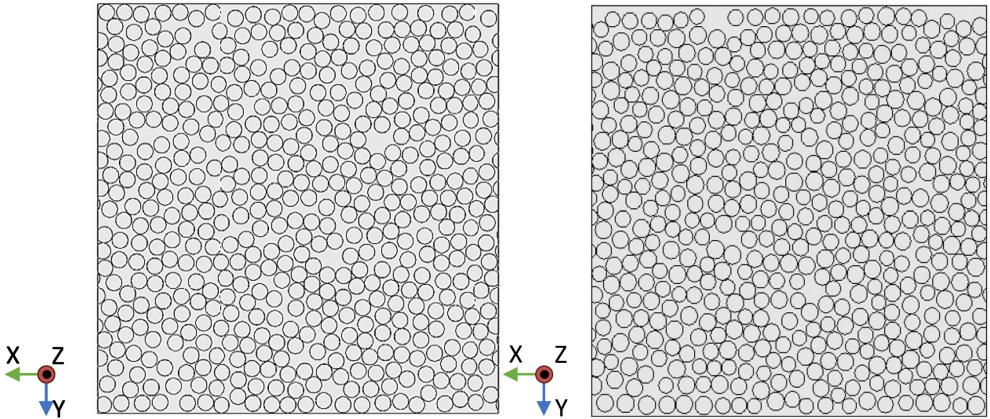

(a) (b)

Figure 5

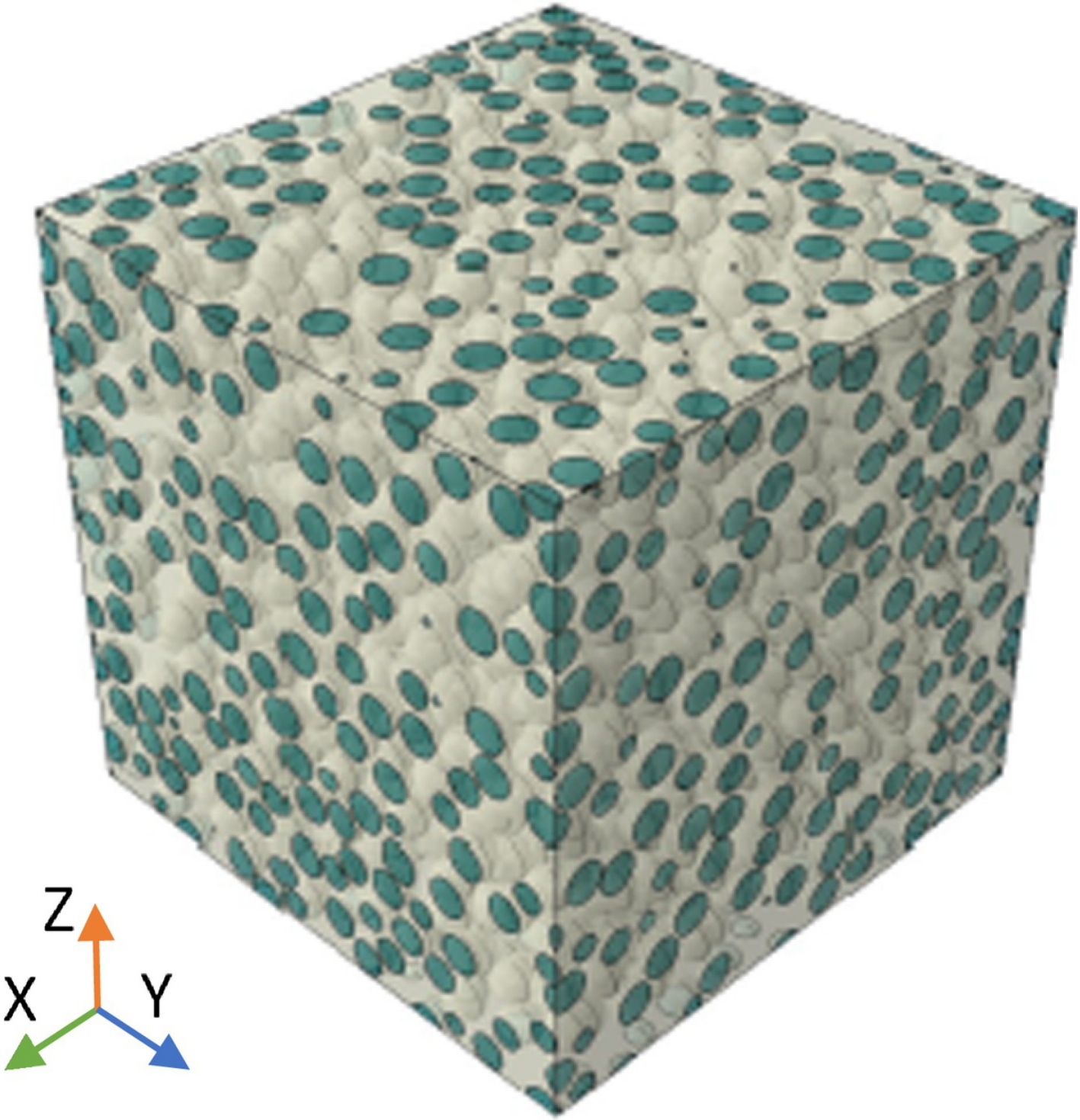

Figure 6

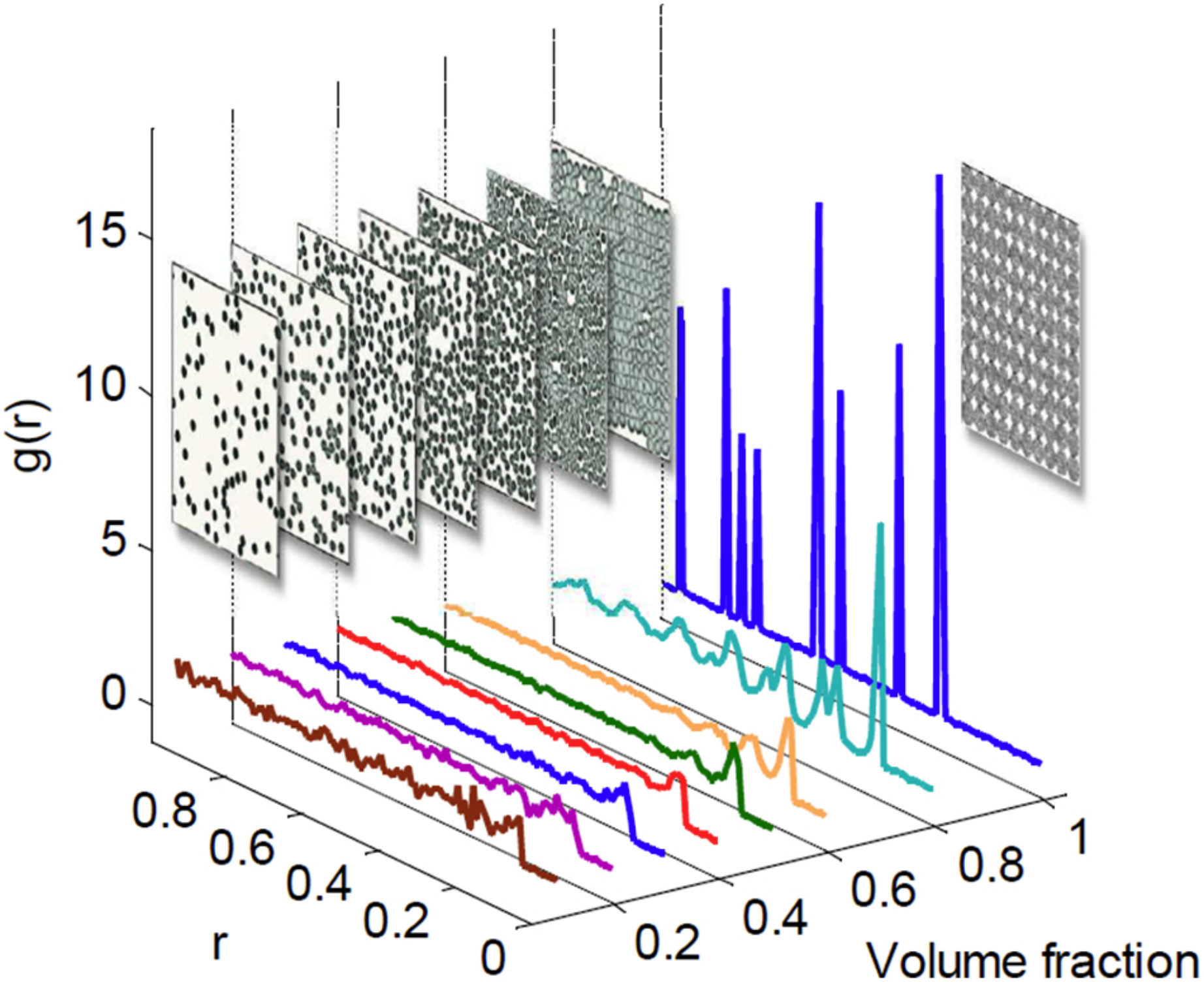

Figure 7

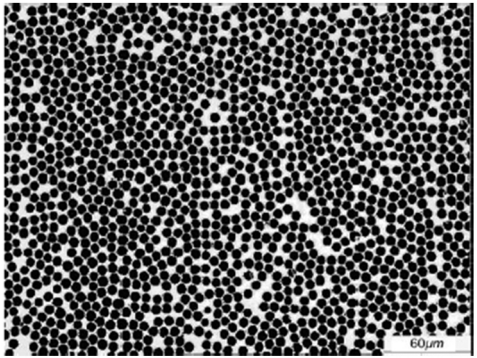
60μm

(a)

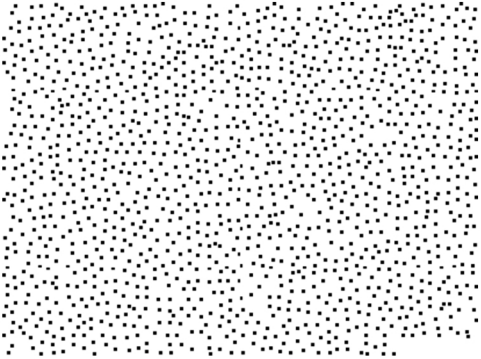

(b)

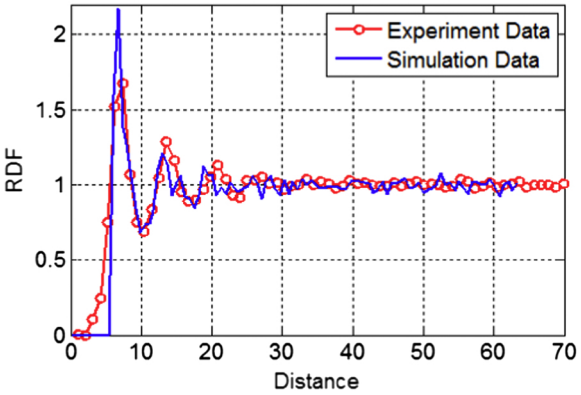
Experiment Data
Simulation Data
RDF
Distance
0
0.5
1
1.5
2
0
10
20
30
40
50
60
70

(c)

Figure 8

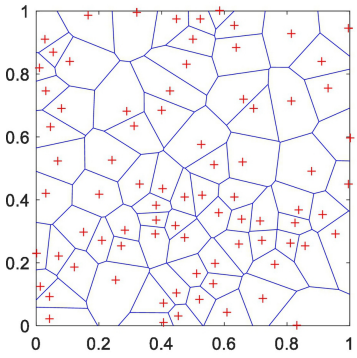

10% volume fraction

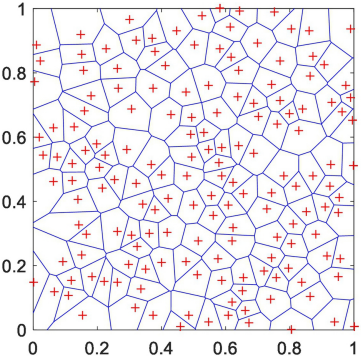

20% volume fraction

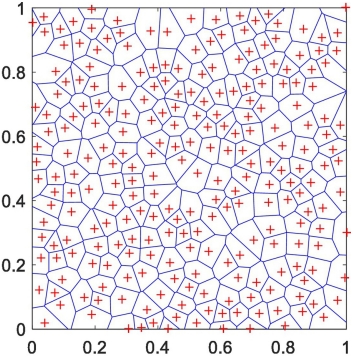

30% volume fraction

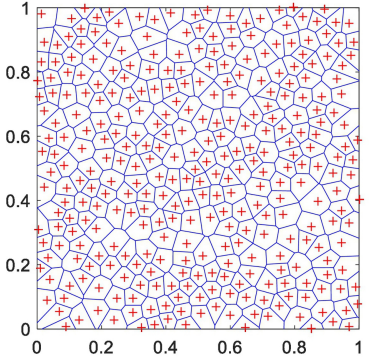

40% volume fraction

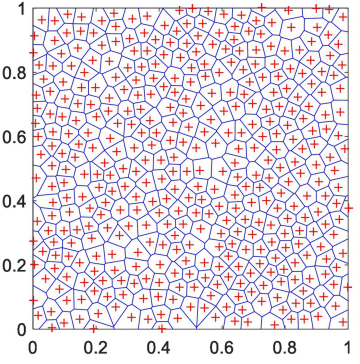

50% volume fraction

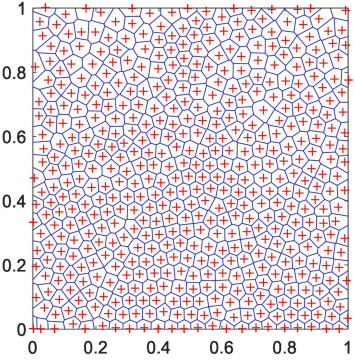

62% volume fraction

Figure 9

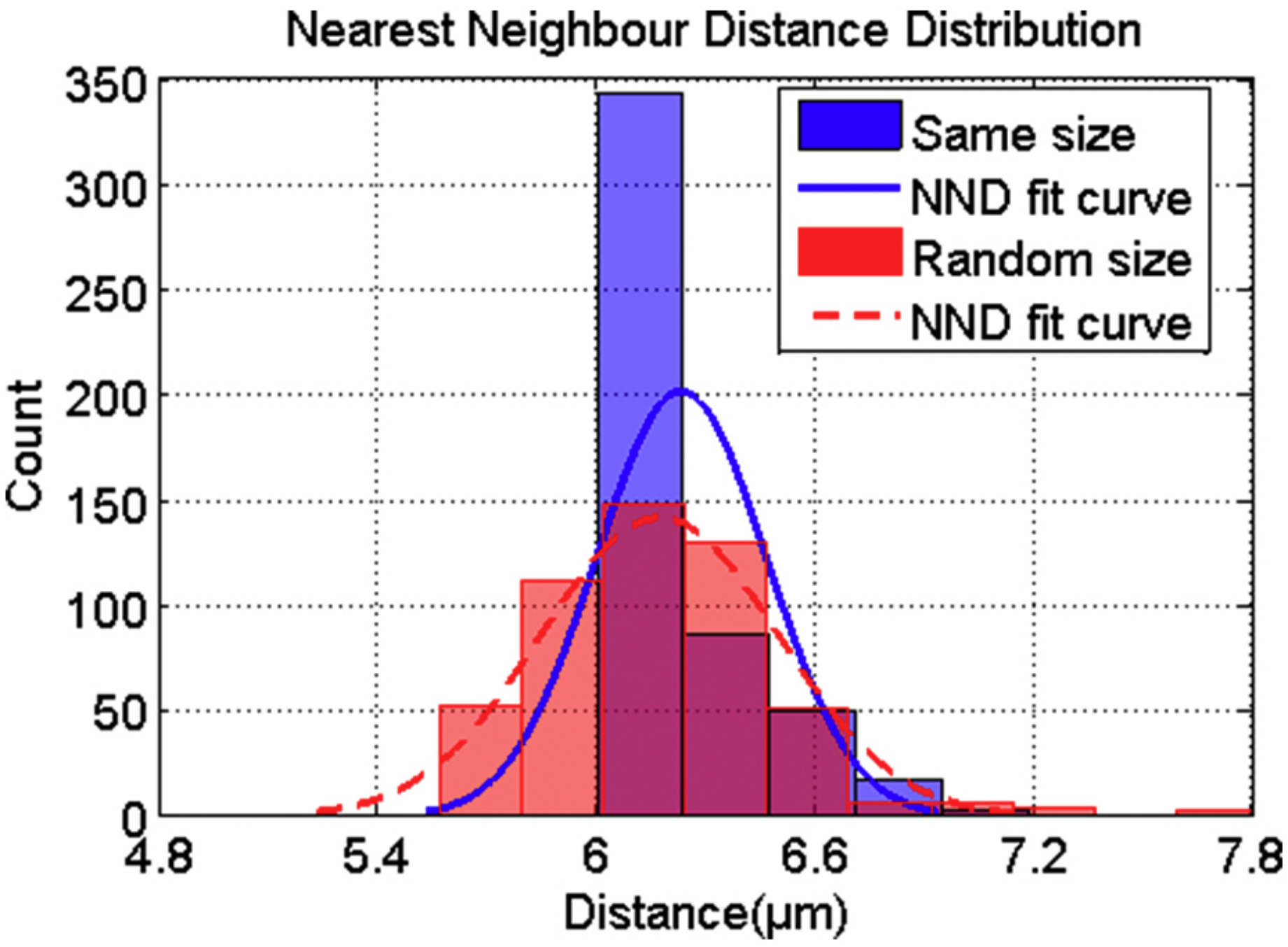
Nearest Neighbour Distance Distribution
Same size
NND fit curve
Random size
NND fit curve
Count
350
300
250
200
150
100
50
0
4.8
5.4
6
6.6
7.2
7.8
Distance(μm)

Figure 10

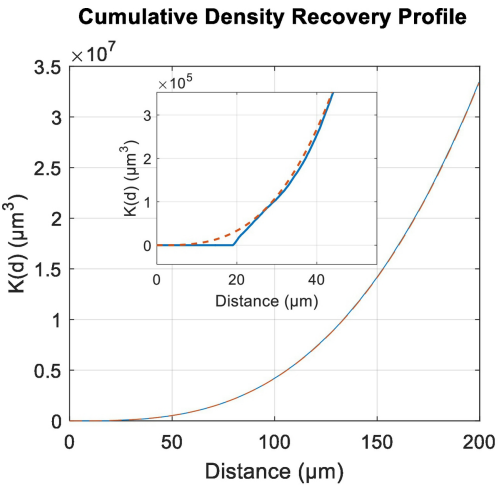

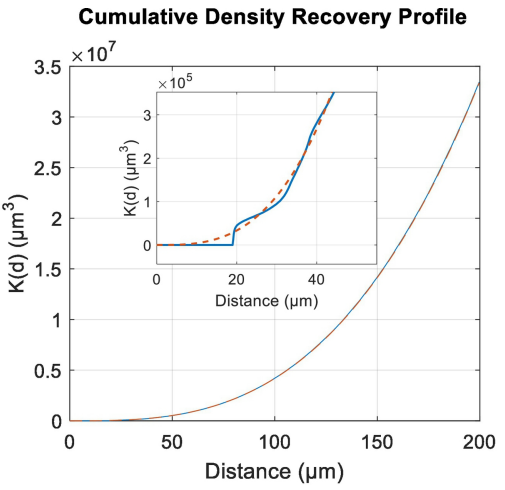

(a) The K-function in 30% (left) and 60% (right) volume fractions

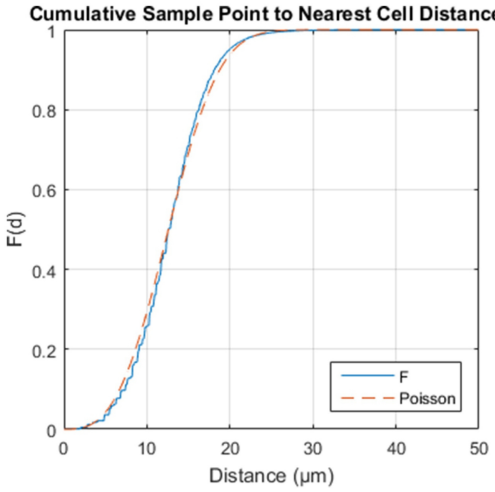

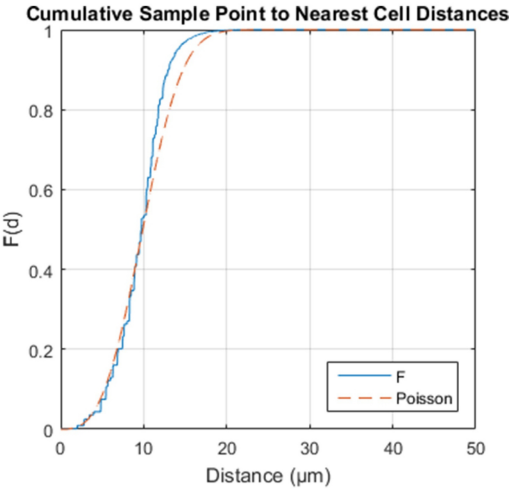

(b) The F-function in 30% (left) and 60% (right) volume fractions

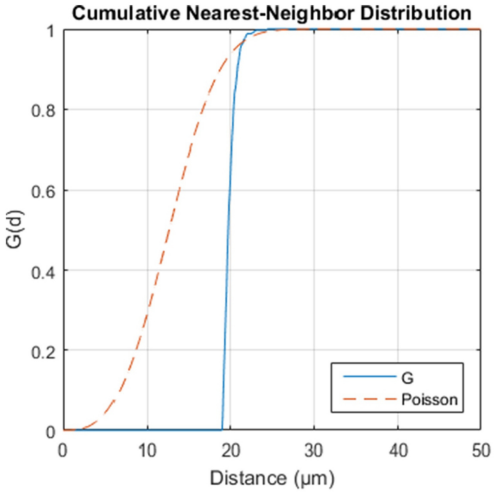

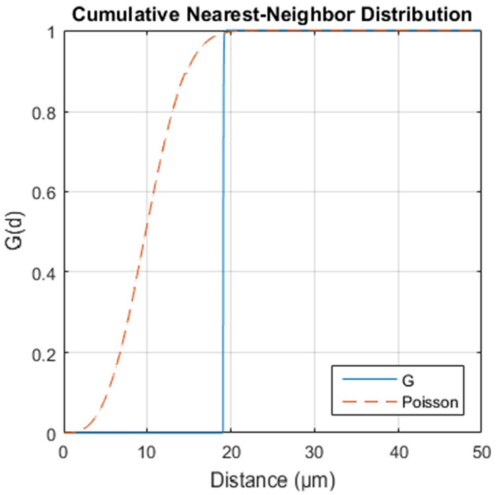

(c) The G-function in 30% (left) and 60% (right) volume fractions

Figure 11

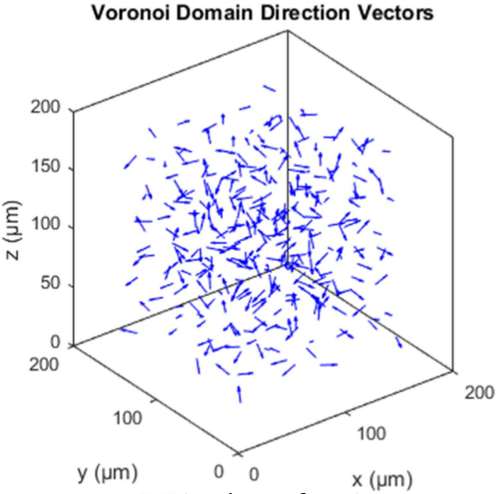

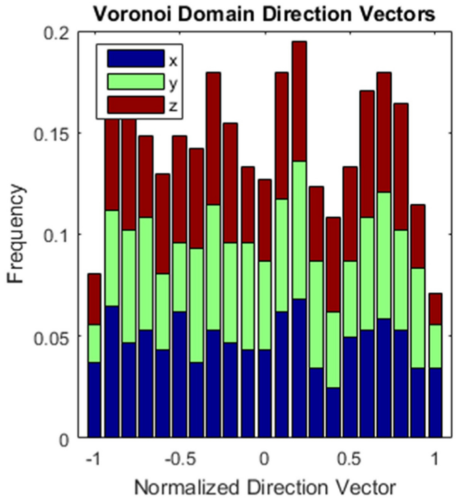

30% volume fraction

(a)

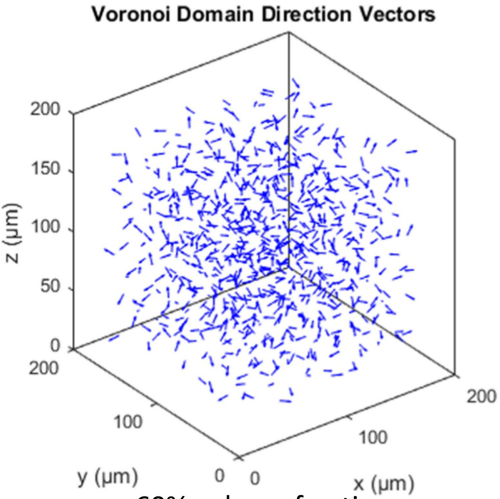

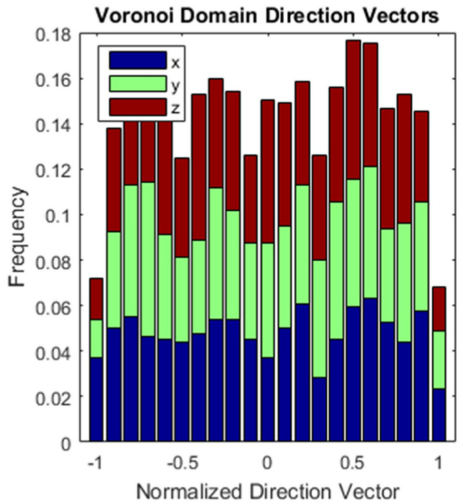

60% volume fraction

(b)

Figure 12

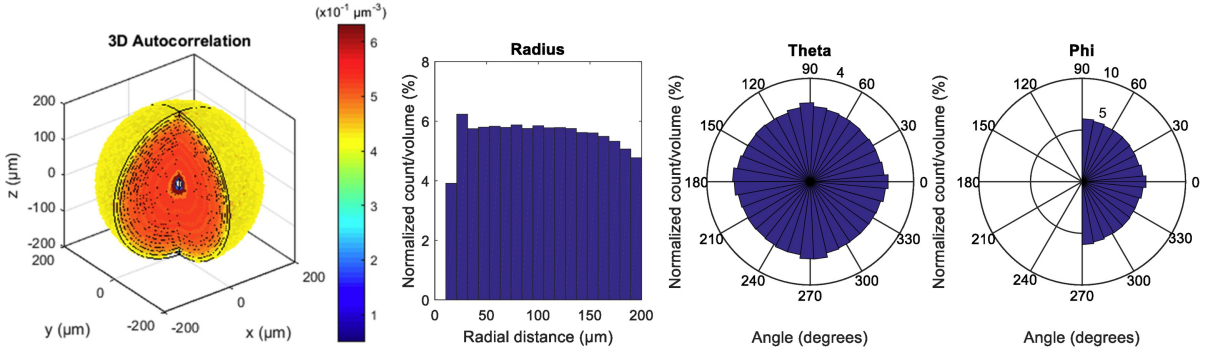

(a)

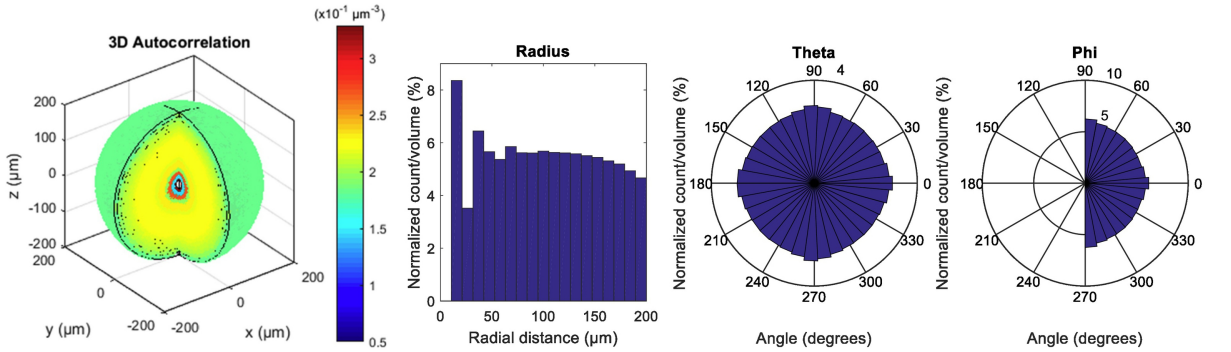

(b)

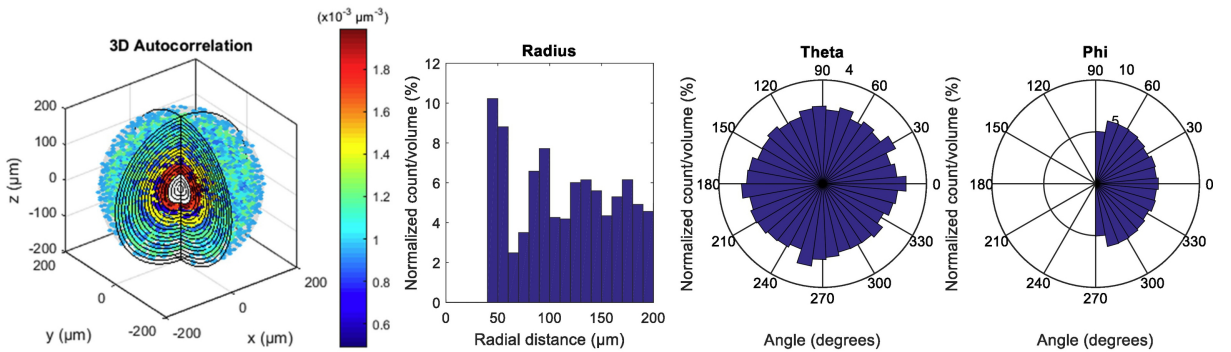

(c)

Figure 13

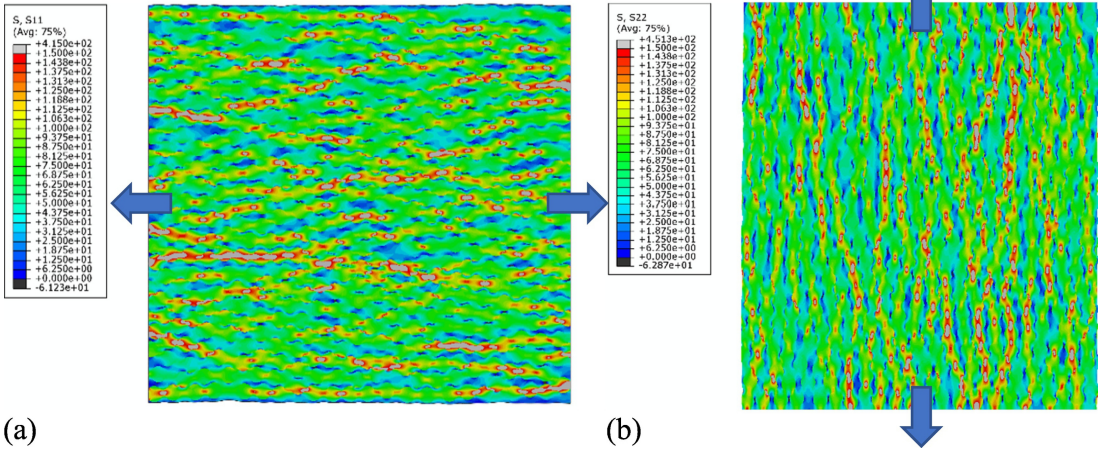
S, S11
(Avg: 75%)
+4.150e+02
+1.500e+02
+1.438e+02
+1.375e+02
+1.313e+02
+1.250e+02
+1.188e+02
+1.125e+02
+1.063e+02
+1.000e+02
+9.375e+01
+8.750e+01
+8.125e+01
+7.500e+01
+6.875e+01
+6.250e+01
+5.625e+01
+5.000e+01
+4.375e+01
+3.750e+01
+3.125e+01
+2.500e+01
+1.875e+01
+1.250e+01
+6.250e+00
+0.000e+00
-6.123e+01
S, S22
(Avg: 75%)
+4.513e+02
+1.500e+02
+1.438e+02
+1.375e+02
+1.313e+02
+1.250e+02
+1.188e+02
+1.125e+02
+1.063e+02
+1.000e+02
+9.375e+01
+8.750e+01
+8.125e+01
+7.500e+01
+6.875e+01
+6.250e+01
+5.625e+01
+5.000e+01
+4.375e+01
+3.750e+01
+3.125e+01
+2.500e+01
+1.875e+01
+1.250e+01
+6.250e+00
+0.000e+00
-6.287e+01
(a)
(b)

Figure 14

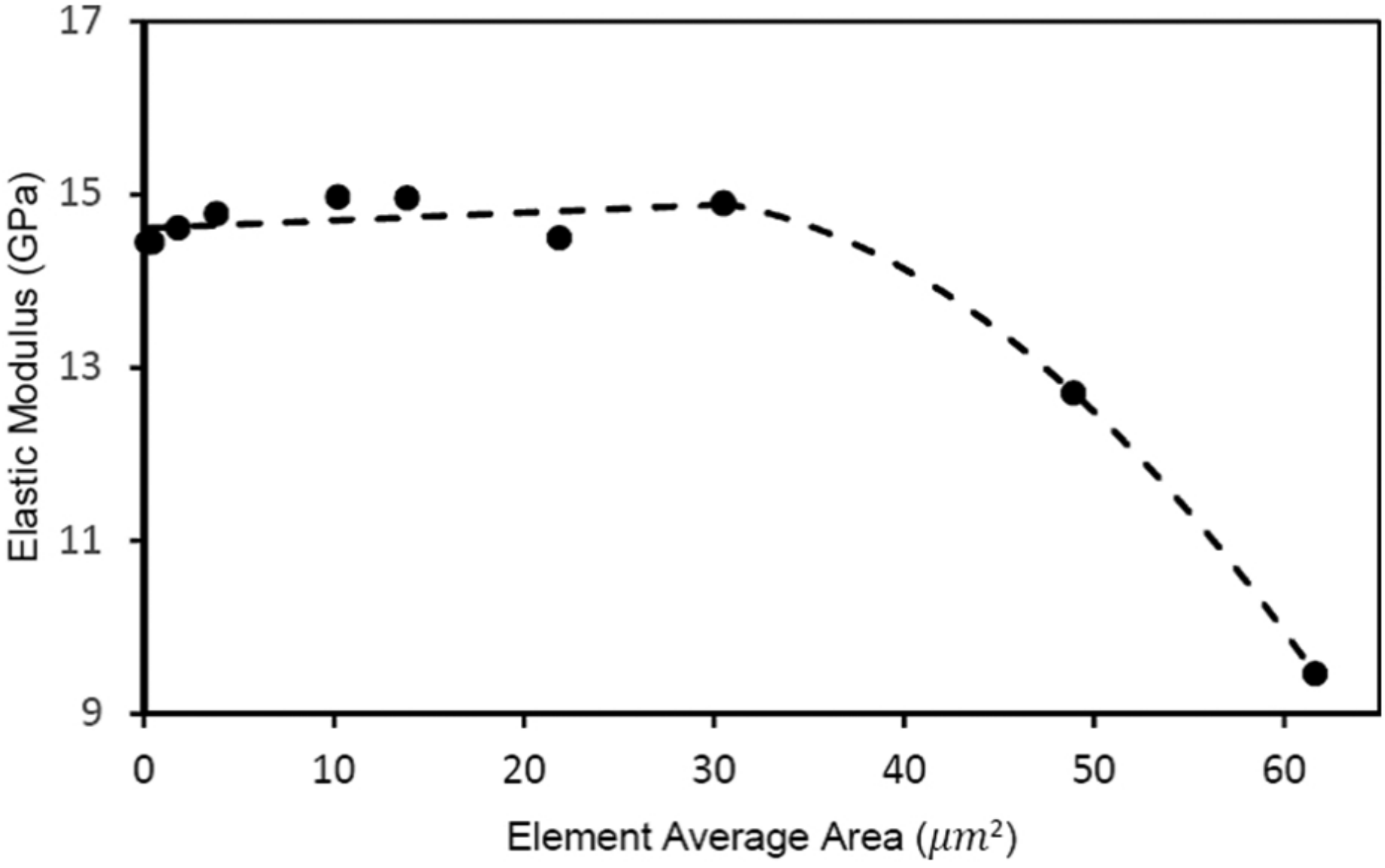
17
15
13
11
9
Elastic Modulus (GPa)
0
10
20
30
40
50
60
Element Average Area (μm^2)

Figure 15

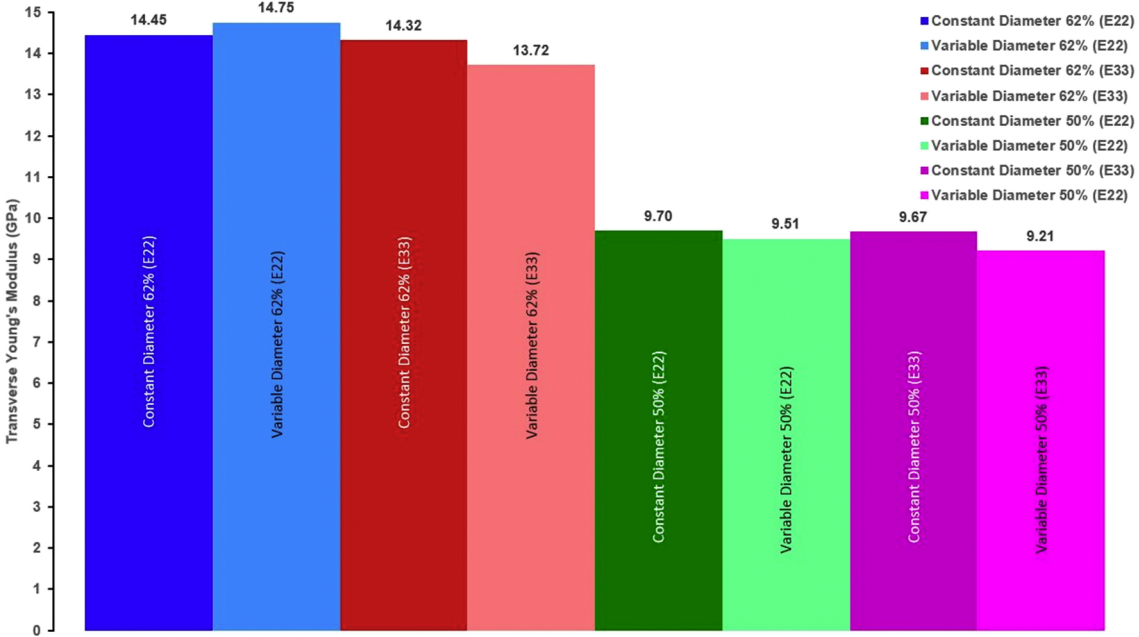
Transverse Young's Modulus (GPa)
0
1
2
3
4
5
6
7
8
9
10
11
12
13
14
15
14.45
14.75
14.32
13.72
9.70
9.51
9.67
9.21
Constant Diameter 62% (E22)
Variable Diameter 62% (E22)
Constant Diameter 62% (E33)
Variable Diameter 62% (E33)
Constant Diameter 50% (E22)
Variable Diameter 50% (E22)
Constant Diameter 50% (E33)
Variable Diameter 50% (E33)
Constant Diameter 62% (E22)
Variable Diameter 62% (E22)
Constant Diameter 62% (E33)
Variable Diameter 62% (E33)
Constant Diameter 50% (E22)
Variable Diameter 50% (E22)
Constant Diameter 50% (E33)
Variable Diameter 50% (E22)

Figure 16

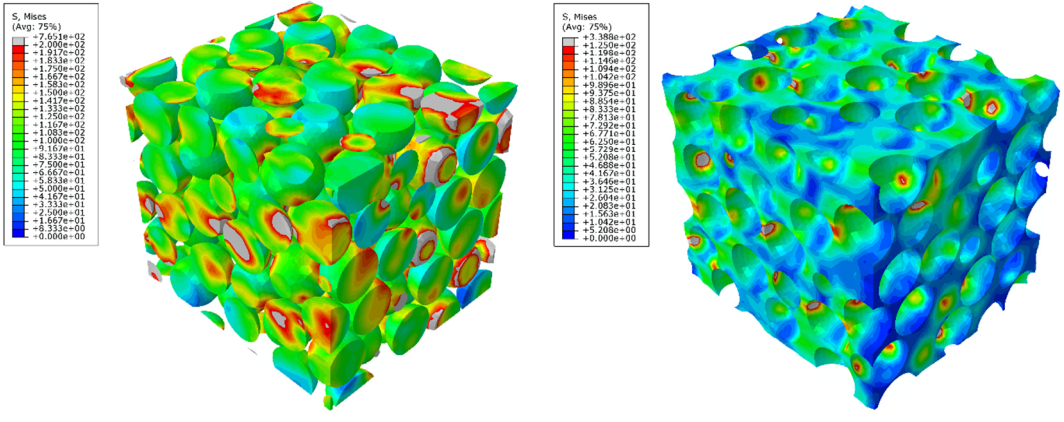
S, Mises
(Avg: 75%)
+7.651e+02
+2.000e+02
+1.917e+02
+1.833e+02
+1.750e+02
+1.667e+02
+1.583e+02
+1.500e+02
+1.417e+02
+1.333e+02
+1.250e+02
+1.167e+02
+1.083e+02
+1.000e+02
+9.167e+01
+8.333e+01
+7.500e+01
+6.667e+01
+5.833e+01
+5.000e+01
+4.167e+01
+3.333e+01
+2.500e+01
+1.667e+01
+8.333e+00
+0.000e+00
S, Mises
(Avg: 75%)
+3.388e+02
+1.250e+02
+1.198e+02
+1.146e+02
+1.094e+02
+1.042e+02
+9.896e+01
+9.375e+01
+8.854e+01
+8.333e+01
+7.813e+01
+7.292e+01
+6.771e+01
+6.250e+01
+5.729e+01
+5.208e+01
+4.688e+01
+4.167e+01
+3.646e+01
+3.125e+01
+2.604e+01
+2.083e+01
+1.563e+01
+1.042e+01
+5.208e+00
+0.000e+00

Figure 17

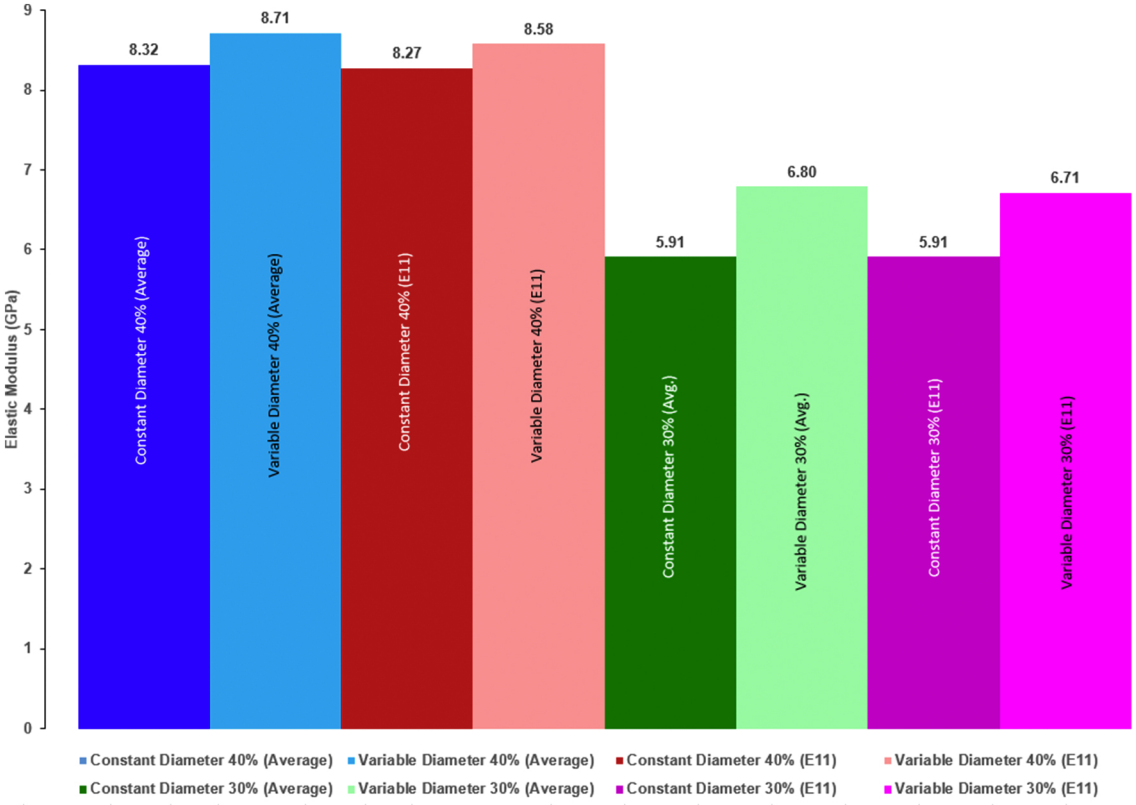
Elastic Modulus (GPa)
0
1
2
3
4
5
6
7
8
9
8.32
8.71
8.27
8.58
5.91
6.80
5.91
6.71
Constant Diameter 40% (Average)
Variable Diameter 40% (Average)
Constant Diameter 40% (E11)
Variable Diameter 40% (E11)
Constant Diameter 30% (Avg.)
Variable Diameter 30% (Avg.)
Constant Diameter 30% (E11)
Variable Diameter 30% (E11)
Constant Diameter 40% (Average)
Variable Diameter 40% (Average)
Constant Diameter 40% (E11)
Variable Diameter 40% (E11)
Constant Diameter 30% (Average)
Variable Diameter 30% (Average)
Constant Diameter 30% (E11)
Variable Diameter 30% (E11)

Figure 18